SYSTEMATIC STUDY OF ERROR SOURCES IN SUPERSONIC SKIN-FRICTION BALANCE MEASUREMENTS

Jerry M. Allen

Langley Research Center
Hampton, Va. 23665

0134049

1. Report No. NASA TN D-8291	2. Government Accession No.	3. Recipient's Catalog No.
4. Title and Subtitle SYSTEMATIC STUDY OF ERROR SOURCES IN SUPERSONIC SKIN-FRICTION BALANCE MEASUREMENTS		5. Report Date October 1976
		6. Performing Organization Code
7. Author(s) Jerry M. Allen		8. Performing Organization Report No. L-10619
9. Performing Organization Name and Address NASA Langley·Research Center Hampton, VA 23665		10. Work Unit No. 505-11-15-02
		11. Contract or Grant No.
12. Sponsoring Agency Name and Address National Aeronautics and Space Administration Washington, DC 20546		13. Type of Report and Period Covered Technical Note
		14. Sponsoring Agency Code

15. Supplementary Notes

16. Abstract

An experimental study has been performed to investigate potential error sources in data obtained with a self-nulling, moment-measuring, skin-friction balance. The balance was installed in the sidewall of a supersonic wind tunnel, and independent measurements of the three forces contributing to the balance output (skin friction, lip force, and off-center normal force) were made for a range of gap size and element protrusion. The relatively good agreement between the balance data and the sum of these three independently measured forces validated the three-term model used in this study.

No advantage to a small gap size was found; in fact, the larger gaps in the present study were preferable. Perfect element alinement with the surrounding test surface resulted in very small balance errors. However, if small protrusion errors are unavoidable, no advantage was found in having the element slightly below the surrounding test surface rather than above it.

17. Key Words (Suggested by Author(s)) Skin-friction balance Turbulent boundary layer Skin-friction measurement errors Supersonic flow	18. Distribution Statement Unclassified – Unlimited Subject Category 34

19. Security Classif. (of this report) Unclassified	20. Security Classif. (of this page) Unclassified	21. No. of Pages 50	22. Price* $3.75

SYSTEMATIC STUDY OF ERROR SOURCES IN SUPERSONIC

SKIN-FRICTION BALANCE MEASUREMENTS

Jerry M. Allen
Langley Research Center

SUMMARY

An experimental study has been performed to investigate potential error sources in data obtained with a self-nulling, moment-measuring, skin-friction balance. The balance was installed in the sidewall of a supersonic wind tunnel, and independent measurements of the three forces contributing to the balance output (skin friction, lip force, and off-center normal force) were made for a range of gap size and element protrusion. The relatively good agreement between the balance data and the sum of these three independently measured forces validated the three-term model used in this study.

No advantage to a small gap size was found. In fact, in the present study the balance was less sensitive to protrusion errors with larger gaps. Thus the ideal of the smallest practical gap size seems unjustified by the present results.

Perfect element alinement with the surrounding test surface resulted in very small balance errors. However, if small protrusion errors are unavoidable, no advantage was found in having the element slightly below the surrounding test surface rather than above it. Positive and negative protrusions of the same magnitude were equally damaging.

INTRODUCTION

The floating-element skin-friction balance is a basic research tool employed in experimental boundary-layer flow studies. Since it is the only instrument which directly measures skin friction, its applications are numerous. For example, balance measurements form the standard by which indirect skin-friction measuring techniques are calibrated. Many widely used skin-friction "theories" rely on correlations with experimental skin-friction balance data. More recently, advanced numerical boundary-layer calculation techniques generally rely on comparisons of calculated skin friction with balance measurements to provide verification.

Because of this fundamental importance of the skin-friction balance in studies of viscous fluid mechanics, it is essential that balance results be made as free of error as possible. There is therefore a need for a systematic investigation of potential error sources in balance measurements. Surprisingly little information on this subject exists in the literature. The probable reason is that most balances available for general use are too small to allow installation of the instrumentation needed to investigate potential error sources.

To investigate these error sources systematically, a large balance was recently constructed at the Langley Research Center and was tested in the thick turbulent boundary layer on the sidewall of a large wind tunnel. The tests were conducted at a free-stream Mach number of 2.19 and at several Reynolds numbers. However, the general results and conclusions obtained in this experiment should be applicable over a wide range of flow conditions. This balance is essentially a large-scale version of the small Kistler balance (see ref. 1), with a scale factor of 14:1. The Kistler balance has been widely used for many years for skin-friction measurements.

SYMBOLS

U.S. Customary Units were employed for the experimental measurements in this study, but the International System of Units (SI) is used herein to report the results.

A	surface area of floating element, $\frac{\pi}{4} D^2$
a	distance from surface of floating element to moment center, 79.38 mm (see fig. 1)
b	moment arm of net normal force acting on surface of floating element (see fig. 1)
C_f	friction force coefficient, $\dfrac{\text{Friction force}}{q_e A}$
C_ℓ	lip force coefficient, $\dfrac{\text{Lip force}}{q_e A}$
C_N	normal force coefficient, $\dfrac{\text{Normal force}}{q_e A}$
C_p	Preston tube pressure coefficient, $\dfrac{p_{pt} - p_w}{q_e}$

C_t total force coefficient, $\dfrac{\text{Total force}}{q_e A}$

c   lip thickness of floating element, 6.35 mm (see fig. 1)

D   diameter of floating element

F   force on element

G   gap size between floating element and surrounding test surface (see fig. 2)

M   Mach number

p   pressure

q   dynamic pressure

R_g universal gas constant

R_θ Reynolds number based on momentum thickness

T   temperature

y   distance normal to test surface (see fig. 4)

z   protrusion, vertical distance between surface of floating element and surrounding test surface (see fig. 2)

γ ratio of specific heats

δ boundary-layer total thickness, 76 mm in this paper

δ^* boundary-layer displacement thickness

θ boundary-layer momentum thickness

μ viscosity

τ shearing stress

ϕ angular location of pressure orifice on surface or lip of floating element, relative to upstream direction

Subscripts:

av   average value

aw   adiabatic wall

e   boundary-layer edge

f   friction

ℓ lip

N   normal

o   evaluated at $z/\delta = 0$

pt   Preston tube

t   total

w   wall

ANALYSIS OF THE PROBLEM

Figure 1 shows a sketch of the sensing element of a moment-measuring balance, such as the one used in this study, and indicates the three aerodynamic forces, friction force, lip force, and normal force, which could contribute to the output of the balance. The net aerodynamic moment about the balance pivot point is obtained by summing the moments created by the individual forces. Thus,

$$\text{Aerodynamic moment} = F_f a + F_\ell \left(a - \frac{c}{2}\right) + F_N b \qquad (1)$$

During balance calibration the moment created by the balance to restore the element to the null position is calibrated against a known total force F_t applied in the streamwise direction on the element surface. Thus,

$$\text{Restoring moment} = F_t a \qquad (2)$$

During testing the aerodynamic moment is counterbalanced by the restoring moment; thus, equations (1) and (2) may be equated to give

$$F_t a = F_f a + F_\ell \left(a - \frac{c}{2}\right) + F_N b \qquad (3)$$

In coefficient form, equation (3) becomes

$$C_t = C_f + \left(1 - \frac{c}{2a}\right)C_\ell + \frac{b}{a}\, C_N \qquad (4)$$

The last two terms in equation (4), representing the lip and normal forces, are normally assumed to be zero in most experiments using skin-friction balances. Thus the total force measured by these balances is usually assumed to be the friction force, and no corrections are applied. By examining these two terms individually, the validity of the usual assumption of negligibility may be assessed, and specific conditions under which the assumption may not be appropriate may be identified.

The first term, lip force, is constant under ideal conditions of no flow through the gap between the floating element and the surrounding test surface. In this case the pressures around the lip of the element are constant, and no net force is created on the lip; that is, $(1 - c/2a)C_\ell = 0$. If there is flow through the gap, the pressures around the lip need not be constant, and a net force in the streamwise direction could be created which would, of course, alter the total output of the balance. This lip force could be a function of both the size of the gap surrounding the element and the protrusion of the element above or below the surrounding test surface. Since this force acts at about the center of the lip, its moment arm is slightly less than that of the friction force, which acts on the surface. For the balance used in this study, the moment arm reduction is about 4 percent; that is, $(1 - c/2a) = 0.96$.

The second term, normal force, is zero if the pressures on the surface and underside of the floating element are constant. In this case, no net force in the normal direction is produced; that is, $(b/a)C_N = 0$. Even if the pressure distribution produces a net force acting at the center of the element, this force does not affect the balance output since $b = 0$ for this case. For an uneven pressure distribution, however, which produces a normal force acting off center, a moment is produced which contributes to the balance output. Again, this normal force could be affected by gap size and protrusion.

Since the two balance geometric parameters which could affect the negligibility of the two force terms discussed in this section are gap size and element protrusion, these two parameters were systematically varied to investigate their effects on the terms in equation (4). To determine the relative magnitudes of the three terms in equation (4) contributing to the total balance output, independent measurements of each term are needed. The test apparatus and techniques employed to provide these measurements are described in the following sections.

TEST APPARATUS AND PROCEDURES

Wind Tunnel

The investigation was conducted in the Langley 4-foot supersonic pressure tunnel, which is described in reference 2. This facility is a rectangular, closed test-section, single-return wind tunnel with provisions for control of pressure, temperature, and humidity of the enclosed air. Two flexible walls of the two-dimensional nozzle can be adjusted to give Mach numbers from 1.4 to 2.6. The maximum operating stagnation pressure is about 2 atm (1 atm = 0.1013 MN/m^2), and the normal operating temperature is about 43° C. The test section is about 1.22 m wide, 1.22 m high, and 2.13 m long.

Test Station

The tunnel sidewall was used as the test surface in this investigation to provide a long run of turbulent flow and a thick boundary layer. The test station was located on the wall center line at about the center of the test section, and was about 4.2 m downstream of the nozzle throat. The permanent model support mechanism was located well downstream of the test station and was traversed to the opposite side of the test section to insure that no flow disturbances originating from the mechanism could affect the data taken during this test.

This tunnel, as described previously, has a two-dimensional nozzle. The upper and lower walls are contoured to produce supersonic flow. The sidewalls, one of which was used as the test surface, are flat from the nozzle throat to the downstream edge of the test section.

Flow Conditions

This investigation was conducted primarily at a free-stream Mach number of 2.19, a free-stream stagnation temperature of 43° C, and a free-stream stagnation pressure of 0.34 atm. Some additional data were obtained at pressures of 1.02 and 1.70 atm to assess Reynolds number effects. The sidewall recovery temperature was within a few degrees of ambient temperature outside the tunnel; thus, this test was conducted under conditions of negligible heat transfer.

A pitot-pressure rake located about 5.35 cm downstream of the element was used to monitor the sidewall boundary layer during the several days of testing required to generate the data in this investigation. Pitot profiles obtained from this rake (with the balance

element at zero protrusion) were combined with the local static pressure to yield Mach number profiles, with the usual assumptions of constant static pressure and total temperature throughout the boundary layer. These profiles are listed in table I. The boundary-layer thickness varied somewhat with Reynolds number. The variation, however, was small. Thus, for the purpose of nondimensionalizing parameters in this paper, the boundary-layer thickness was assumed to be constant and equal to 76 mm.

Integral thicknesses were calculated from these pitot-pressure data. The following table lists the flow conditions of this test, including the mean values of the integral parameters of the sidewall boundary layer. In the table, T_t is stagnation temperature, p_t is stagnation pressure, and R is the free-stream unit Reynolds number.

p_t, atm	R, m^{-1}	θ, cm	δ^*, cm	R_θ
0.34	3.61×10^6	0.450	1.66	1.62×10^4
1.02	10.73	.358	1.30	3.84
1.70	17.72	.337	1.22	5.97

$$M_e = 2.19, \quad T_t = 43^\circ \text{ C}, \quad T_w/T_{aw} = 1.0$$

Skin-Friction Balance

Details of the design and construction of the balance used in this study can be found in reference 3. Basically, the balance is a self-nulling, moment-measuring device whose sensing element is pivoted to rotate in response to forces in the streamwise direction. Any moment on the element created by aerodynamic forces tending to rotate the element is balanced internally by an opposite moment produced by an electrically created force. The output of the balance is simply the voltage required to keep the sensing element in the null position.

Figure 2 shows sketches of the test apparatus and the geometric parameters which were systematically varied. For the balance measurements, interchangeable floating elements of different diameter were used to test the effect of gap size. The diameter of the balance opening was 12.7 cm, and the gap widths G were varied from about 0.1 to 1.0 percent of this value by use of these interchangeable floating elements. A drive mechanism controlled the protrusion of the floating elements relative to the surrounding test surface. The boundary layer at the test station was about 76 mm thick. The floating elements were protruded about ±1.7 percent of this value.

Lip Pressure

Figure 3 shows sketches illustrating the methods employed to evaluate the aerodynamic forces acting on the floating element. The pressure distribution around the lip of the element was recorded at the same time that the balance measurements were made. The lip pressure orifices shown in figure 2 were 0.4 mm in diameter and were spaced 22.5° apart around the rim. The pressure inside the chamber of the balance was assumed to be constant at and below the lower edge of the lip, and a linear pressure distribution was assumed to exist between the lower edge of the lip and the surface of the element. The vertical and circumferential pressure distributions on the lip are thus defined, and the net force on the lip is simply the integration of this distribution in the streamwise direction over the area of the lip.

Surface Pressure

The normal force contribution to the balance output was measured with a pressure-instrumented element the same size as the largest balance element. Hence normal force estimates over the protrusion range could be obtained for only one gap size (G/D = 0.001). This dummy element had pressure orifices 0.4 mm in diameter located at 14 radial locations on the element surface (see fig. 3). At each protrusion the element was rotated through 360° in small increments so that detailed pressure distributions over the entire element surface were recorded. Integration of these pressures and their associated moment arms over the element surface yielded the net normal force contribution. Note that this integration procedure directly produces the product of the normal force F_N and the

moment arm b, which is the form needed in calculating the normal force contribution to the balance output

$$\frac{b}{a} C_N \equiv \frac{b F_N}{a q_e A}$$

Thus, it is not necessary to separate the force and the moment arm; only their product is important.

Preston Tube

The dummy floating element was also used in providing an estimate of the skin-friction variation over the protrusion range by mounting a Preston tube on the element surface. As seen in figure 3, the tip of the Preston tube was located at the center of the element, and the base was mounted over a static pressure orifice,

8

which served to record the pitot pressure. The outside diameter of the Preston tube was 5.0 mm and its inside diameter was 3.0 mm.

The Preston tube skin friction was calculated over the protrusion range from the measured pitot and static pressures according to the following equation:

$$\frac{p_{pt} - p_W}{\tau_W} = 96 + 60 \log_{10}\left(\frac{\bar{R}}{50}\right) + 23.7 \left[\log_{10}\left(\frac{\bar{R}}{50}\right)\right]^2$$

$$+ \frac{\tau_W}{\gamma p_W} 10^4 \left(\bar{R}^{0.3} - 2.38\right) \tag{5}$$

where

$$\bar{R} \equiv \frac{d}{\mu_W} \sqrt{\frac{\tau_W p_W}{R_g T_W}}$$

and d is the outside diameter of the Preston tube. This calibration equation is a slight modification of the Bradshaw-Unsworth equation (see ref. 4). The modification was made to take advantage of more recent and accurate calibration data. The only difference between equation (5) and the Bradshaw-Unsworth equation is in the

last term. The term $(\bar{R}^{0.3} - 2.38)$ in equation (5) has replaced

$(\bar{R}^{0.26} - 2.00)$ in the Bradshaw-Unsworth equation. For the flow conditions of this study the Preston tube skin friction calculated from equation (5) is about 6 percent lower than it would have been had the Bradshaw-Unsworth equation been used.

It should be noted that Preston tubes are themselves calibrated against skin-friction balance measurements. Thus, skin friction obtained from Preston tube data is not completely independent of potential balance errors. It is believed, however, that balance errors are small in the data on which equation (5) was based. In any event the Preston tube data in this study were obtained to estimate the variation in skin friction over the protrusion range. Any balance errors included in the Preston tube calibration equation could have a small effect on the magnitude of the skin friction, but would have little effect on its variation.

Boundary-Layer Rake

A 14-tube pitot-pressure rake was located immediately downstream of the balance to monitor the sidewall boundary layer and to assure that no large changes occurred in the boundary layer during the several days of this investigation. The tips of the 14 tubes in the rake were located 15.58 cm downstream of the center of the floating element, or 5.32 cm downstream of the element trailing edge. A check run was made with the rake removed to verify that the presence of the rake had no influence on the balance data. A schematic sketch of the rake can be found in figure 4.

The integral parameters, θ and δ^*, were computed from the rake data when the balance element was at zero protrusion. Since the flow was at zero pressure gradient and zero heat transfer, the usual assumptions of constant static pressure and total temperature throughout the boundary layer were made. The scatter among the integral parameters at zero protrusion for different test runs at different gap sizes ranged from about ±3.0 percent at the highest unit Reynolds number to about ±4.5 percent at the lowest.

It was estimated that the integral thicknesses at the center of the floating element were about 2 percent less than those measured by the rake because of the slightly downstream location of the rake. Since this percentage is within the scatter of the measured data, no corrections were made, and the integral thicknesses given in the previous table are assumed to apply at the center of the element.

DISCUSSION OF RESULTS

Presentation of Data

Reynolds number effects were investigated for only the total force and lip force data, which are presented in figures 5 and 6 for all the protrusions, gap sizes, and Reynolds numbers investigated. These data are also listed in tables II and III. Positive protrusion indicates that the element is above the surrounding test surface, whereas negative protrusion indicates recession below the test surface. Also, positive force coefficients are in the downstream direction, whereas negative coefficients are in the upstream direction. Examination of these figures reveals that the effects of Reynolds number are relatively minor except for the smallest gap size. Hence, figures 5 and 6 are presented only for completeness and are not examined in detail. Instead, the result at

$R_\theta = 1.62 \times 10^4$ is selected for more detailed examination in subsequent sections of this paper and for comparison with the normal

10

force and Preston tube skin-friction results, which were also obtained at this Reynolds number.

Total Force

Figure 7 shows the effects of protrusion and gap size on the total force measured by the balance. At zero protrusion the effect of gap size is very small. The average of these zero-protrusion total force measurements ($C_{t,o,av}$ = 0.00158) is the value with which other force coefficients in this paper are compared. Thus, all coefficients presented hereafter have been normalized by $C_{t,o,av}$ so that the magnitude of the forces can be more easily ascertained.

Protrusion has a strong effect on the total force. Note that large forces were measured at relatively small ratios of protrusion to boundary-layer thickness. Small protrusion errors, therefore, which would be negligible in thick boundary-layer experiments, could become important in thin boundary-layer experiments.

Figure 7 shows trends which are contradictory to two intuitive assumptions usually held by researchers using skin-friction balances. One is that small gaps are preferable to larger ones since a smaller gap better simulates a smooth, continuous surface without discontinuities. Figure 7 reveals, however, that the balance is much more sensitive to protrusion errors at the smaller gap sizes. The second assumption is that small element recession below the surrounding test surface is much preferable to a comparable protrusion above the test surface. Figure 7 reveals, however, that for the same gap size, small amounts of positive and negative protrusion are equally damaging to the accuracy of the balance.

The effect of gap size on total force at zero protrusion, as noted previously, is small compared with its effect with protrusion. These zero-protrusion data are shown in figure 8 plotted as a function of gap size. Within the scatter of the data, very little effect of gap size on total force coefficient is shown.

Shown for comparison in figure 8 are data obtained with small Kistler balances tested at the same location on the tunnel sidewall and at the same flow conditions as the large balance. As described previously the Kistler balance is essentially a small-scale (1:14) version of the large balance. The data from the Kistler balances have been plotted at their gap-to-diameter ratio, which is rather large because of the small size of their elements. In terms of absolute size, however, the gap on the Kistler balances is about the same as the smallest gap used on the large balance, about 0.1 mm. This value is approximately the smallest practical size

that can be used on balances of this type. Note that there is more
scatter in the Kistler data than in the large balance data, although
the overall agreement between the two is good.

Also shown in figure 8 is the value of C_f calculated from the
measured R_θ with the Spalding-Chi theory. This quasi-theoretical
C_f value is in good agreement with the experimental data.

Lip Force

Figure 9 shows sample pressure distributions around the lip
for the smallest gap tested (G/D = 0.001) over the range of pro-
trusion. The data for z/δ = 0.017 show higher pressures upstream
than downstream, indicating a positive net force on the lip. On the
other hand, the data at z/δ = -0.017 show higher pressures down-
stream, indicating a negative net force on the lip. For zero pro-
trusion the pressure distribution was virtually constant, indicating
a very small net lip force.

These pressure distributions were integrated over the area of
the lip as described previously to yield the net forces on the lip
over the range of protrusion and gap size, and the results are
shown in figure 10. In general, positive protrusion results in
positive lip forces, whereas negative protrusion results in negative
lip forces. The lip forces are more sensitive to protrusion errors
at the smaller gap sizes, a trend which was also noticed in the
total force results of figure 7. Note that all lip forces are small
at zero protrusion.

Normal Force

Normal force results were obtained only at the smallest gap
size (G/D = 0.001). Figure 11 shows sample pressure contours over
the surface of the element at the maximum negative protrusion
(z/δ = -0.017). Low pressure regions near the leading edge and
high pressure regions near the trailing edge result in a center of
pressure located on the downstream side of the element. A moment
is thus produced on the element tending to rotate it in the down-
stream direction, that is, in the direction of a positive drag
force.

A comparison of the pressure distributions on the element sur-
face for different protrusions can be seen in figure 12, in which
the pressures around the outer edge of the element - but still on
the surface, not the lip - are shown. The curve for z/δ = -0.017
is taken from the data of figure 11. The pressure difference
between the upstream and downstream edges of the element is much

greater for negative protrusion; hence the moment produced at this protrusion is larger than at the other protrusions. Note that the pressure distribution for perfect alinement ($z/\delta = 0$) is virtually constant, indicating a very small moment. Also, the two peaks which occur for $z/\delta = 0.017$ contribute very little to the moment on the element since they occur along the axis of rotation (near $\phi = 90^{\circ}$ and 270°).

The pressures over the entire surface and their associated moment arms were integrated as described previously to yield the normal force contribution to the balance output. Figure 13 shows the results of these integrations and confirms the previous observation that the normal force contribution is much larger for negative protrusion than for positive protrusion. The normal force results for all three Reynolds numbers R_{θ} are listed in table IV.

Skin Friction

Figure 14 shows the skin-friction variation over the protrusion range measured by the Preston tube mounted on the surface of the dummy floating element. Preston tube results were obtained only at the smallest gap size ($G/D \boxempty 0.001$). The fact that the variation shown in figure 14 is rather small throughout the z/δ range is not surprising since the variation of shearing stress in the lower part of a boundary layer is known to be small. At zero protrusion the Preston tube skin friction is about 6 percent lower than the balance total force reading. The Preston tube skin friction for all three Reynolds numbers R_{θ} is listed in table V.

Comparison of Terms

The three terms which contribute to the balance measurement — skin friction, lip force, and off-center normal force — have now been independently measured for the same gap size and Reynolds number over the protrusion range and can now be compared. Figure 15 shows this comparison, where the data were taken from figures 10, 13, and 14. The heavy solid line represents the sum of these three terms.

Figure 16 shows how this sum compares with the direct balance measurements, which were taken from figure 7. The good agreement shown validates the three-term model used in this study and gives confidence that the relative magnitudes of these three terms over the protrusion range, as shown in figure 15, are approximately correct.

Comparison With O'Donnell's Results

In reference 5, O'Donnell presents skin-friction balance results for a range of positive and negative protrusion. The balance used in O'Donnell's study operated on a different principle than the ones used in the present study. O'Donnell's balance contained a spring-loaded element which translated fore and aft within the circular opening surrounding the element in response to the axial force on the element. The balance output was determined by the location of the element within the circular opening. Hence the output was sensitive only to axial force, and not to normal force.

Figure 17 contains a comparison between results from the present balance (interpolated from fig. 7) and results from the balance used in reference 5 at similar Mach number, Reynolds number based on momentum thickness, and gap-to-diameter ratio. In nondimensionalizing O'Donnell's data, the output of his balance at perfect alinement was used for $C_{t,o,av}$, and his boundary-layer thickness was used for δ. It can be seen from figure 17 that the sensitivity of the present balance to protrusion is much larger than that of O'Donnell's balance, and that the trends with negative protrusion are opposite.

Note from figure 17 that O'Donnell's balance has a smaller lip-to-diameter ratio than the present balance. Thus the lip force contribution to O'Donnell's results is probably small since the lip pressures have a small area on which to act. Hence the trend of O'Donnell's data with protrusion probably represents the sum of the skin friction and a small amount of lip force. To check this trend with the data of the present balance, note in the data of figure 15 that if the normal force contribution to the present results is eliminated and the lip force contribution greatly reduced, a trend very similar to that in O'Donnell's data is obtained.

CONCLUSIONS

An experimental study has been performed to investigate potential error sources in data obtained with a self-nulling, moment-measuring, skin-friction balance. The balance was installed in the sidewall of a supersonic wind tunnel, and independent measurements of the three forces contributing to the balance output (skin friction, lip force, and off-center normal force) were made for a range of gap size and element protrusion. On the basis of results of this study the following conclusions are drawn:

1. Because of the agreement shown between the direct balance measurements and the sum of the three independently measured terms

contributing to the balance output, the three-term model for the forces acting on the element is validated.

2. No advantage to a small gap size was found. In fact, in the present study the balance was less sensitive to protrusion errors with larger gaps. Thus the ideal of the smallest practical gap size seems unjustified by the present results.

3. Perfect element alinement with the surrounding test surface resulted in very small balance errors. However, if small protrusion errors are unavoidable, no advantage was found in having the element slightly below the surrounding test surface rather than above it. Positive and negative protrusions of the same magnitude were equally damaging.

4. Since the lip and normal force errors in the present data were so large for relatively small protrusions, efforts in balance design to minimize these errors should be made.

Langley Research Center
National Aeronautics and Space Administration
Hampton, VA 23665
August 18, 1976

REFERENCES

1. Paros, Jerome M.: Application of the Force-Balance Principle to Pressure and Skin Friction Sensors. 16th Annual Technical Meeting Proceedings, Inst. Environmental Sci., 1970, pp. 363-368.

2. Schaefer, William T., Jr.: Characteristics of Major Active Wind Tunnels at the Langley Research Center. NASA TM X-1130, 1965.

3. Fowke, James G.: Development of a Skin-Friction Balance To Investigate Sources of Error in Direct Skin-Friction Measurements. M.S. Thesis, Univ. of Virginia, 1969

4. Bradshaw, P.; and Unsworth, K.: A Note on Preston Tube Calibrations in Compressible Flow. IC Aero Rep. 73-07. Dep. Aeronaut., Imperial College Sci. & Technol., Sept. 1973.

5. O'Donnell, Francis B., Jr.: A Study of the Effect of Floating-Element Misalignment on Skin-Friction-Balance Accuracy. DRL-515, CR-10 (Contract NOrd-16498), Univ. of Texas, Mar. 3, 1964.

TABLE I.- MACH NUMBER PROFILES IN BOUNDARY LAYER

y, mm	M for R_θ of -		
	1.62×10^4	3.84×10^4	5.97×10^4
0	0	0	0
2.54	1.045	1.210	1.267
5.59	1.227	1.388	1.436
8.89	1.363	1.498	1.519
15.24	1.529	1.618	1.654
21.59	1.650	1.741	1.763
27.94	1.756	1.862	1.898
34.29	1.857	1.973	2.008
40.64	1.966	2.057	2.096
46.99	2.078	2.145	2.148
53.34	2.136	2.183	2.178
59.69	2.161	2.196	2.190
66.04	2.174	2.197	2.191
72.39	2.179	2.197	2.192
76.96	2.182	2.198	2.192

TABLE II.- TOTAL FORCE RESULTS

(a) $R_\theta = 1.62 \times 10^4$

z, mm	C_t for G/D of -					
	0.001	0.002	0.004	0.006	0.008	0.010
-1.270	0.00602	0.00580	0.00563	0.00507	0.00472	0.00396
-1.016	.00452	.00427	.00420	.00388	.00365	.00312
-.762	.00308	.00286	.00298	.00286	.00280	.00258
-.508	.00190	.00172	.00211	.00212	.00226	.00219
-.254	.00128	.00132	.00163	.00178	.00191	.00183
-.127	.00127	.00134	.00154	.00169	.00178	.00166
-.102	.00131	.00138	.00153	.00167	.00174	.00163
-.076	.00137	.00141	.00152	.00165	.00172	.00162
-.051	.00142	.00146	.00152	.00163	.00170	.00159
-.025	.00149	.00150	.00152	.00161	.00166	.00158
0	.00158	.00157	.00153	.00160	.00164	.00157
.025	.00168	.00165	.00156	.00160	.00162	.00155
.051	.00179	.00175	.00158	.00161	.00161	.00155
.076	.00190	.00184	.00163	.00162	.00161	.00155
.102	.00201	.00196	.00167	.00162	.00162	.00155
.127	.00212	.00206	.00172	.00163	.00163	.00157
.254	.00278	.00267	.00213	.00183	.00178	.00170
.508	.00403	.00388	.00317	.00268	.00236	.00215
.762	.00507	.00493	.00425	.00374	.00322	.00281
1.016	.00588	.00575	.00517	.00475	.00417	.00371
1.270	.00657	.00653	.00600	.00552	.00501	.00457

TABLE II.- Continued

(b) $R_\theta = 3.84 \times 10^4$

z, mm	C_t for G/D of -					
	0.001	0.002	0.004	0.006	0.008	0.010
-1.270	0.00584	0.00602	0.00567	0.00607	-------	0.00453
-1.016	.00407	.00427	.00403	.00464	0.00414	.00362
-.762	.00238	.00262	.00257	.00340	.00317	.00313
-.508	.00085	.00117	.00148	.00234	.00261	.00273
-.254	.00017	.00071	.00122	.00168	.00213	.00199
-.127	.00056	.00103	.00137	.00162	.00180	.00168
-.102	.00073	.00112	.00140	.00161	.00173	.00164
-.076	.00087	.00121	.00141	.00157	.00169	.00162
-.051	.00106	.00132	.00142	.00155	.00165	.00157
-.025	.00129	.00142	.00143	.00152	.00162	.00156
0	.00153	.00153	.00145	.00152	.00159	.00153
.025	.00179	.00169	.00147	.00152	.00157	.00153
.051	.00209	.00189	.00152	.00152	.00156	.00153
.076	.00238	.00208	.00159	.00152	.00156	.00154
.102	.00263	.00230	.00167	.00155	.00157	.00155
.127	.00292	.00252	.00178	.00158	.00157	.00157
.254	.00397	.00360	.00257	.00190	.00172	.00164
.508	.00547	.00513	.00432	.00307	.00233	.00206
.762	.00648	.00626	.00563	.00447	.00333	.00291
1.016	-------	-------	.00673	.00567	.00452	.00389
1.270	-------	-------	-------	.00686	.00562	.00498

TABLE II.- Concluded

$$(c) \quad R_\theta = 5.97 \times 10^4$$

z, mm	C_t for G/D of -					
	0.001	0.002	0.004	0.006	0.008	0.010
-1.270	-------	-------	-------	-------	-------	-------
-1.016	0.00394	0.00423	0.00409	-------	-------	0.00385
-.762	.00218	.00256	.00254	0.00348	0.00335	.00340
-.508	.00058	.00103	.00137	.00240	.00287	.00302
-.254	-.00023	.00043	.00111	.00183	.00233	.00214
-.127	.00023	.00090	.00129	.00171	.00194	.00170
-.102	.00037	.00102	.00131	.00168	.00185	.00163
-.076	.00058	.00113	.00132	.00165	.00177	.00160
-.051	.00088	.00125	.00134	.00162	.00172	.00158
-.025	.00118	.00137	.00135	.00157	.00167	.00155
0	.00148	.00148	.00137	.00153	.00162	.00152
.025	.00183	.00167	.00140	.00148	.00157	.00148
.051	.00223	.00191	.00146	.00148	.00156	.00148
.076	.00258	.00213	.00152	.00151	.00156	.00147
.102	.00284	.00240	.00162	.00152	.00156	.00147
.127	.00310	.00267	.00176	.00156	.00156	.00147
.254	-------	.00392	.00261	.00183	.00161	.00142
.508	-------	-------	-------	.00299	.00214	.00187
.762	-------	-------	-------	-------	.00324	.00278
1.016	-------	-------	-------	-------	-------	.00385
1.270	-------	-------	-------	-------	-------	-------

TABLE III.- LIP FORCE RESULTS

(a) $R_\theta = 1.62 \times 10^4$

z, mm	C_ℓ for G/D of -					
	0.001	0.002	0.004	0.006	0.008	0.010
-1.270	-0.00491	-0.00473	-0.00425	-0.00393	-0.00367	-0.00355
-1.016	-.00448	-.00427	-.00386	-.00367	-.00347	-.00335
-.762	-.00384	-.00354	-.00313	-.00318	-.00306	-.00295
-.508	-.00293	-.00253	-.00195	-.00213	-.00218	-.00186
-.254	-.00163	-.00127	-.00076	-.00073	-.00055	-.00033
-.127	-.00084	-.00056	-.00036	-.00027	-.00016	-.00008
-.102	-.00067	-.00042	-.00028	-.00018	-.00010	-.00007
-.076	-.00048	-.00026	-.00022	-.00017	-.00008	-.00006
-.051	-.00031	-.00013	-.00015	-.00016	-.00006	-.00006
-.025	-.00010	.00007	-.00003	-.00013	-.00005	-.00006
0	.00005	.00020	.00003	-.00006	-.00005	-.00005
.025	.00025	.00035	.00014	-.00007	-.00005	-.00006
.051	.00044	.00053	.00024	-.00002	-.00004	-.00008
.076	.00065	.00065	.00029	.00002	-.00004	-.00008
.102	.00080	.00081	.00038	.00003	-.00005	-.00008
.127	.00099	.00095	.00045	.00005	-.00006	-.00009
.254	.00178	.00168	.00084	.00014	-.00014	-.00018
.508	.00315	.00292	.00173	.00056	-.00015	-.00027
.762	.00418	.00387	.00258	.00132	.00027	-.00027
1.016	.00495	.00457	.00325	.00206	.00095	.00020
1.270	.00552	.00515	.00384	.00260	.00151	.00073

TABLE III.- Continued

(b) $R_\theta = 3.84 \times 10^4$

z, mm	C_ℓ for G/D of -					
	0.001	0.002	0.004	0.006	0.008	0.010
-1.270	-0.00616	-0.00560	-0.00495	-0.00466	-0.00433	-0.00415
-1.016	-.00577	-.00528	-.00456	-.00444	-.00414	-.00407
-.762	-.00524	-.00466	-.00394	-.00407	-.00387	-.00378
-.508	-.00435	-.00348	-.00269	-.00346	--------	-.00302
-.254	-.00274	-.00170	-.00052	-.00087	-.00116	-.00062
-.127	-.00156	-.00068	-.00015	-.00006	-.00007	-.00007
-.102	-.00123	-.00049	-.00014	-.00002	.00002	-.00007
-.076	-.00096	-.00033	-.00013	.00001	.00002	-.00007
-.051	-.00056	-.00014	-.00006	.00003	.00002	-.00007
-.025	-.00017	.00006	-.00004	.00001	.00002	-.00007
0	.00016	.00025	.00002	0	.00001	-.00008
.025	.00053	.00045	.00004	-.00002	-.00006	-.00013
.051	.00086	.00069	.00012	-.00007	-.00013	-.00021
.076	.00124	.00089	.00007	-.00012	-.00017	-.00027
.102	.00152	.00109	.00006	-.00016	-.00025	-.00030
.127	.00184	.00130	.00005	-.00018	-.00030	-.00035
.254	.00315	.00232	.00024	-.00058	-.00078	-.00075
.508	.00465	.00374	.00163	-.00064	-.00139	-.00140
.762	.00556	.00458	.00274	.00045	-.00123	-.00157
1.016	--------	--------	.00354	.00145	-.00046	-.00136
1.270	--------	--------	--------	.00217	.00046	-.00075

TABLE III.- Concluded

(c) $R_\theta = 5.97 \times 10^4$

z, mm	C_ℓ for G/D of -					
	0.001	0.002	0.004	0.006	0.008	0.010
-1.270	--------	--------	--------	--------	--------	--------
-1.016	-0.00623	-0.00557	--------	--------	--------	-0.00438
-.762	-.00567	-.00495	-0.00518	-0.00436	-0.00419	-.00410
-.508	-.00480	-.00375	--------	-.00376	-.00354	-.00334
-.254	-.00316	-.00170	-.00044	-.00114	-.00157	-.00088
-.127	-.00174	-.00068	-.00001	.00004	-.00015	-.00008
-.102	-.00148	-.00046	-.00002	.00012	.00003	-.00007
-.076	-.00115	-.00032	-.00004	.00010	.00005	-.00007
-.051	-.00066	-.00015	-.00004	.00009	.00005	-.00007
-.025	-.00025	.00005	-.00003	.00008	.00004	-.00010
0	.00016	.00025	.00002	.00002	.00002	-.00015
.025	.00064	.00045	.00003	-.00003	-.00005	-.00023
.051	.00110	.00067	0	-.00012	-.00017	-.00031
.076	.00150	.00084	-.00010	-.00018	-.00025	-.00037
.102	.00185	.00106	-.00019	-.00027	-.00035	-.00043
.127	.00226	.00131	-.00027	-.00036	-.00046	-.00049
.254	--------	.00238	-.00027	-.00094	-.00104	-.00095
.508	--------	--------	--------	-.00124	-.00178	-.00164
.762	--------	--------	--------	--------	-.00182	-.00187
1.016	--------	--------	--------	--------	--------	-.00180
1.270	--------	--------	--------	--------	--------	--------

TABLE IV.- NORMAL FORCE RESULTS FOR $G/D = 0.001$

R_θ	z, mm	$\frac{b}{a} C_N$
1.62×10^4	-1.270	0.00991
	0	.00020
	1.270	.00027
3.84×10^4	-1.270	0.01144
	-1.016	.00908
	0	.00023
	1.270	.00127
5.97×10^4	-1.270	-------
	0	0.00022
	1.270	.00164

TABLE V.- PRESTON TUBE SKIN FRICTION FOR $G/D = 0.001$

R_θ	z, mm	C_p	C_f
1.62×10^4	-1.270	0.335	0.00142
	-.635	.348	.00146
	0	.361	.00149
	.635	.365	.00152
	1.270	.374	.00155
3.84×10^4	-1.270	0.411	0.00126
	-.635	.433	.00130
	0	.453	.00134
	.635	.464	.00137
	1.270	.473	.00140
5.97×10^4	-1.270	0.447	0.00120
	-.635	.469	.00124
	0	.494	.00128
	.635	.505	.00130
	1.270	.514	.00132
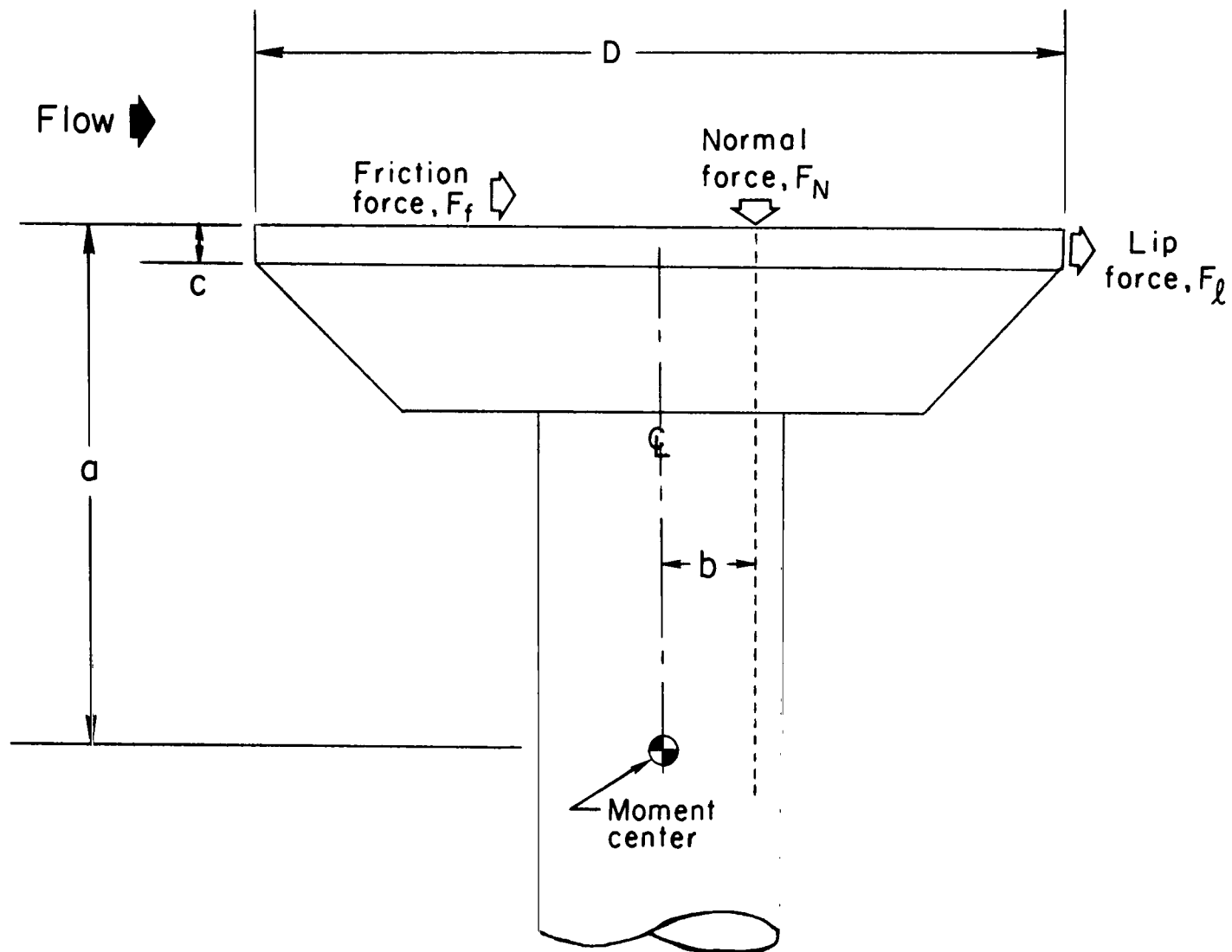
Figure 1.- Floating sensing element and aerodynamic forces acting on it.

Test apparatus

Floating element

Pivot arm

Pressure orifices

Geometric variables

Gap size

$\leftarrow$ G

Protrusion

z
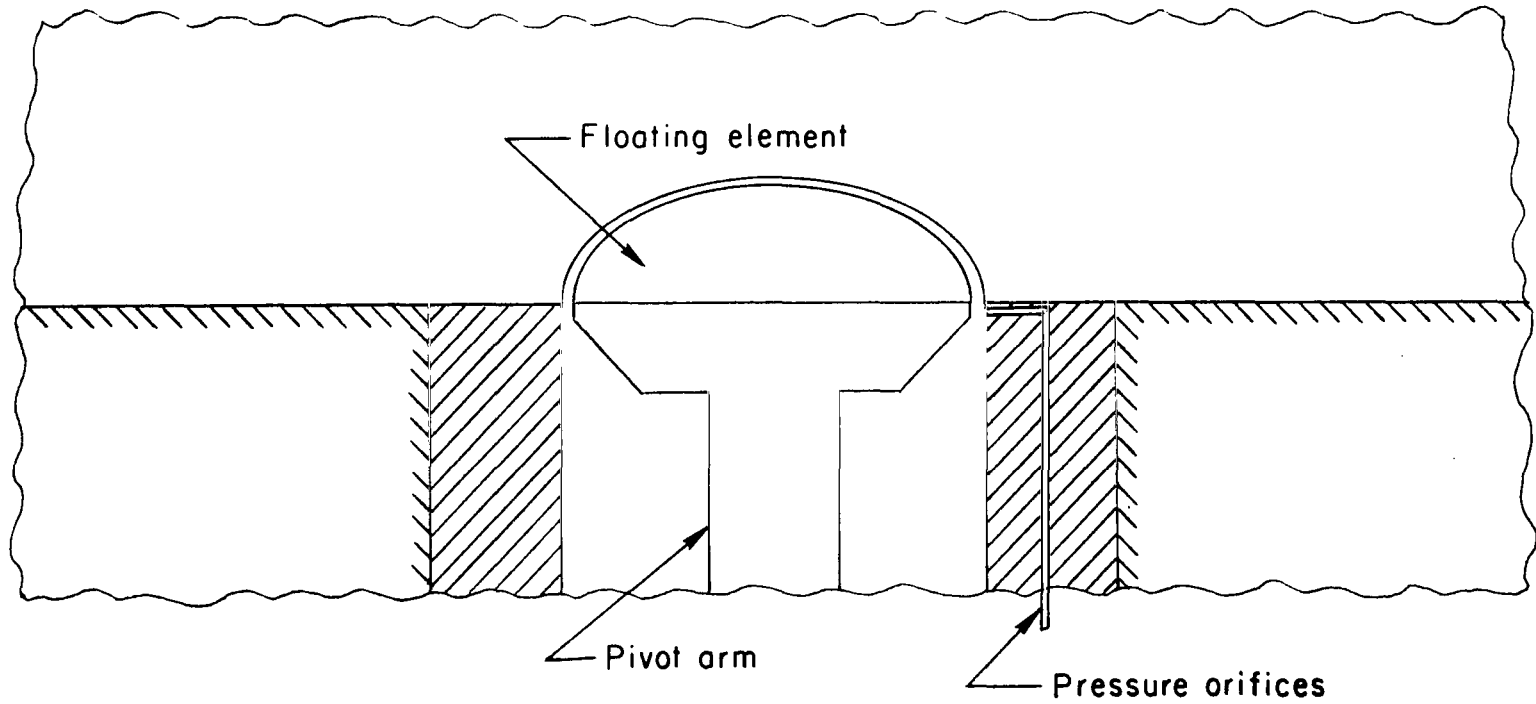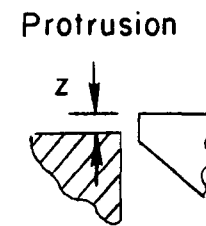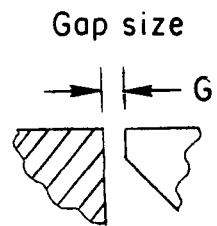
Figure 2.- Test apparatus and geometric variables.

Lip force

F_ℓ

Normal force

F_N

Friction force

F_f

Lip orifices
(located on
balance housing)

Surface
orifices

ϕ

Preston
tube
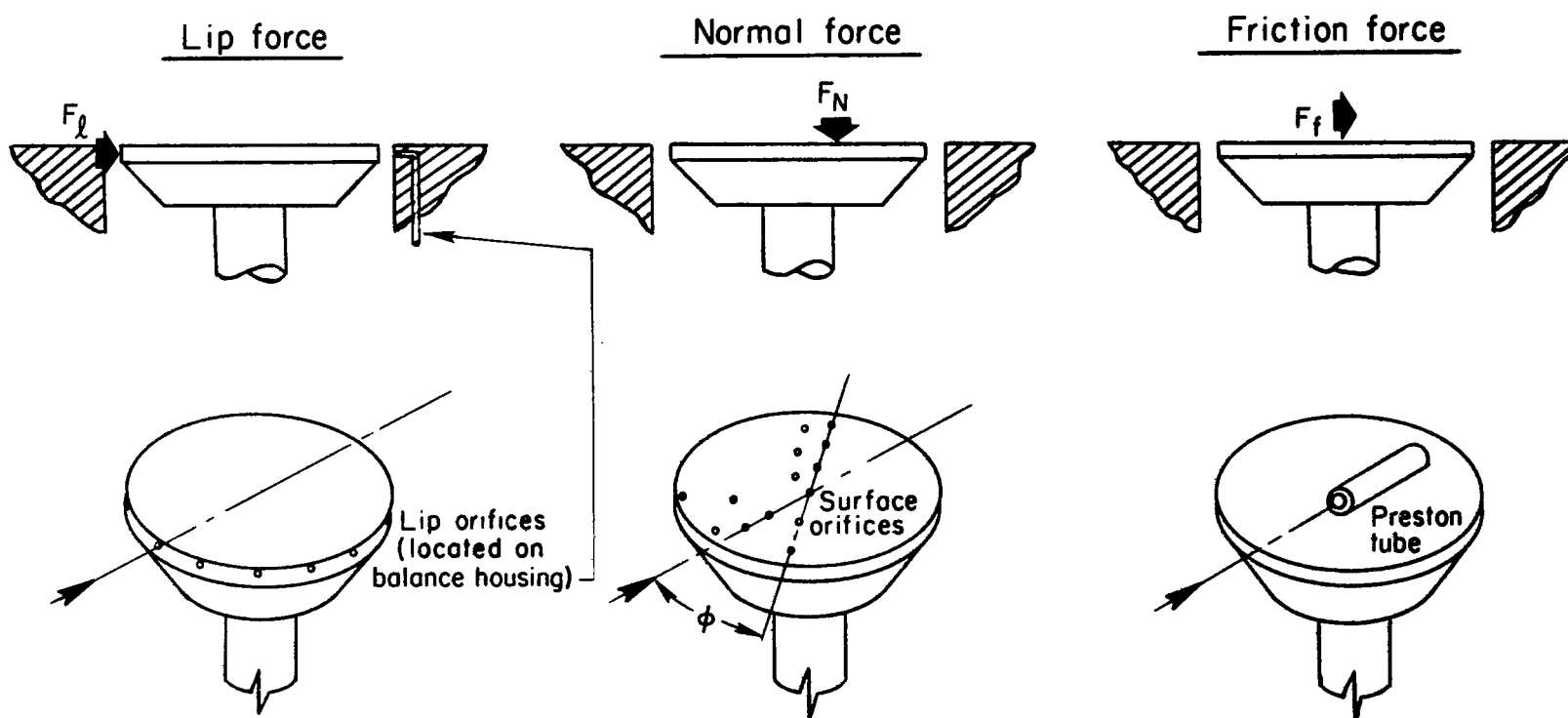
Figure 3.- Methods used to evaluate aerodynamic forces acting on element.
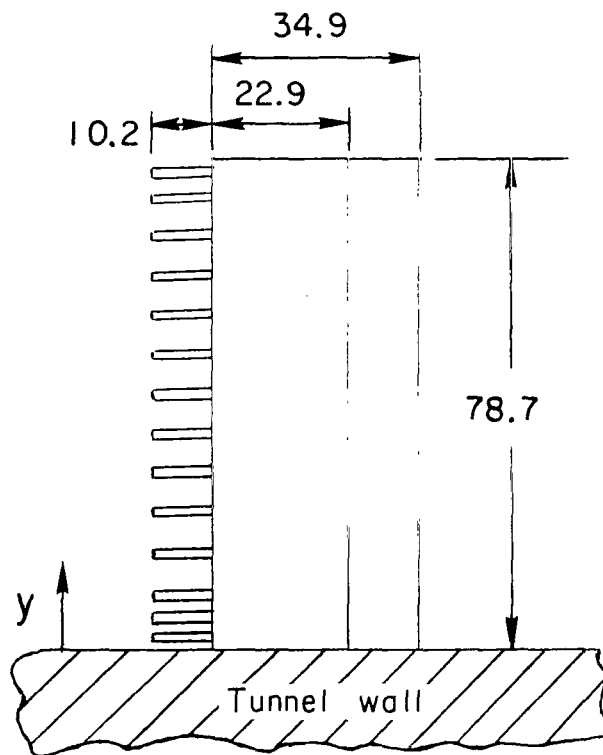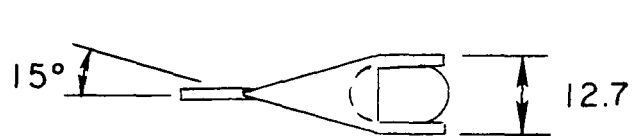
Tube no.	Distance from wall to center of tube
1	2.5
2	5.6
3	8.9
4	15.2
5	21.6
6	27.9
7	34.3
8	40.6
9	47.0
10	53.3
11	59.7
12	66.0
13	72.4
14	77.0

Tube tip details

Shape   Circular
Outside diam 1.0
Inside diam 0.5

Figure 4.- Pitot pressure rake used to monitor boundary layer.
Dimensions are in millimeters.
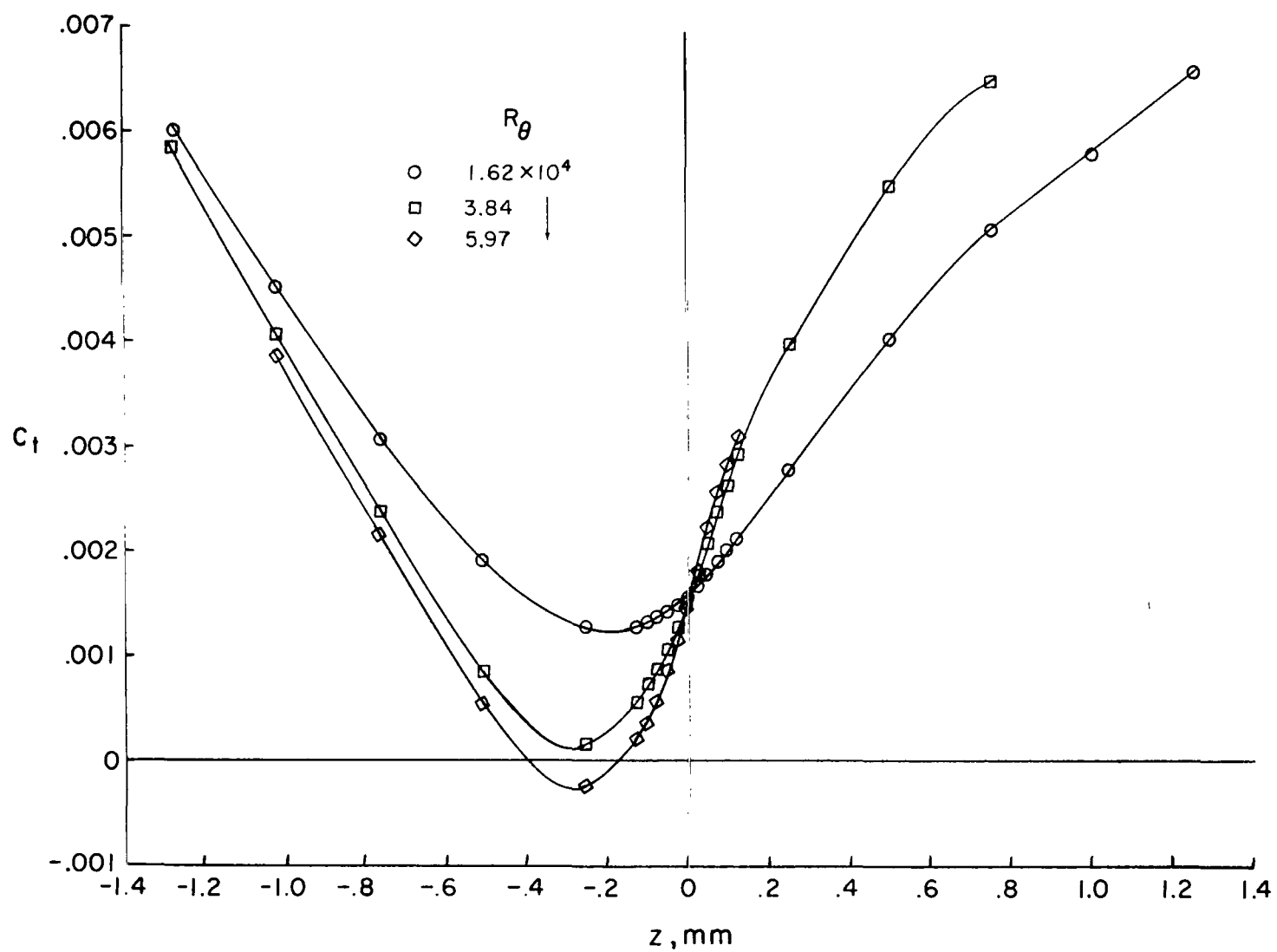
(a) G/D = 0.001.

Figure 5.- Total force results.
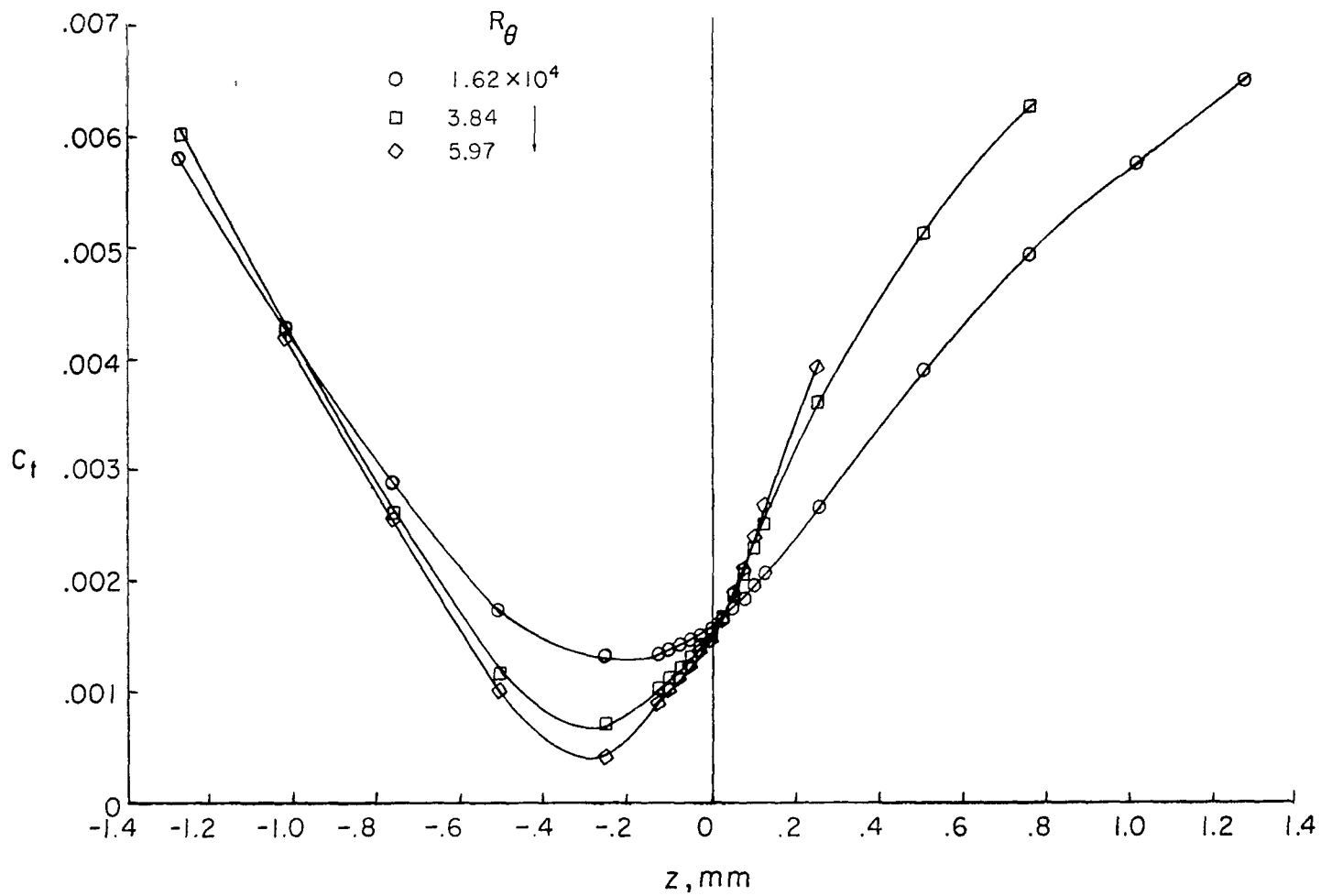
(b) G/D = 0.002.

Figure 5.- Continued.
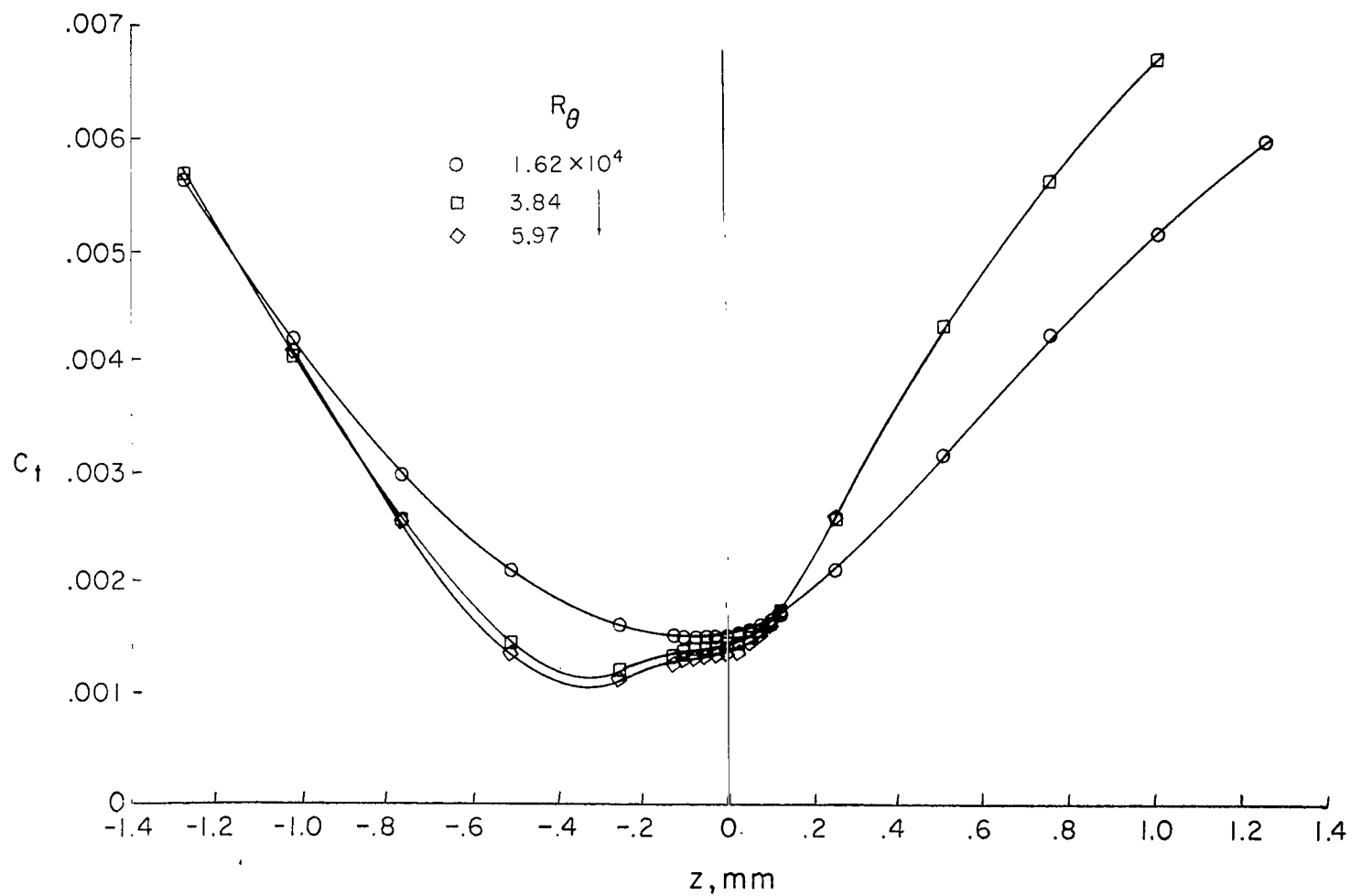
(c) G/D = 0.004.

Figure 5.- Continued.
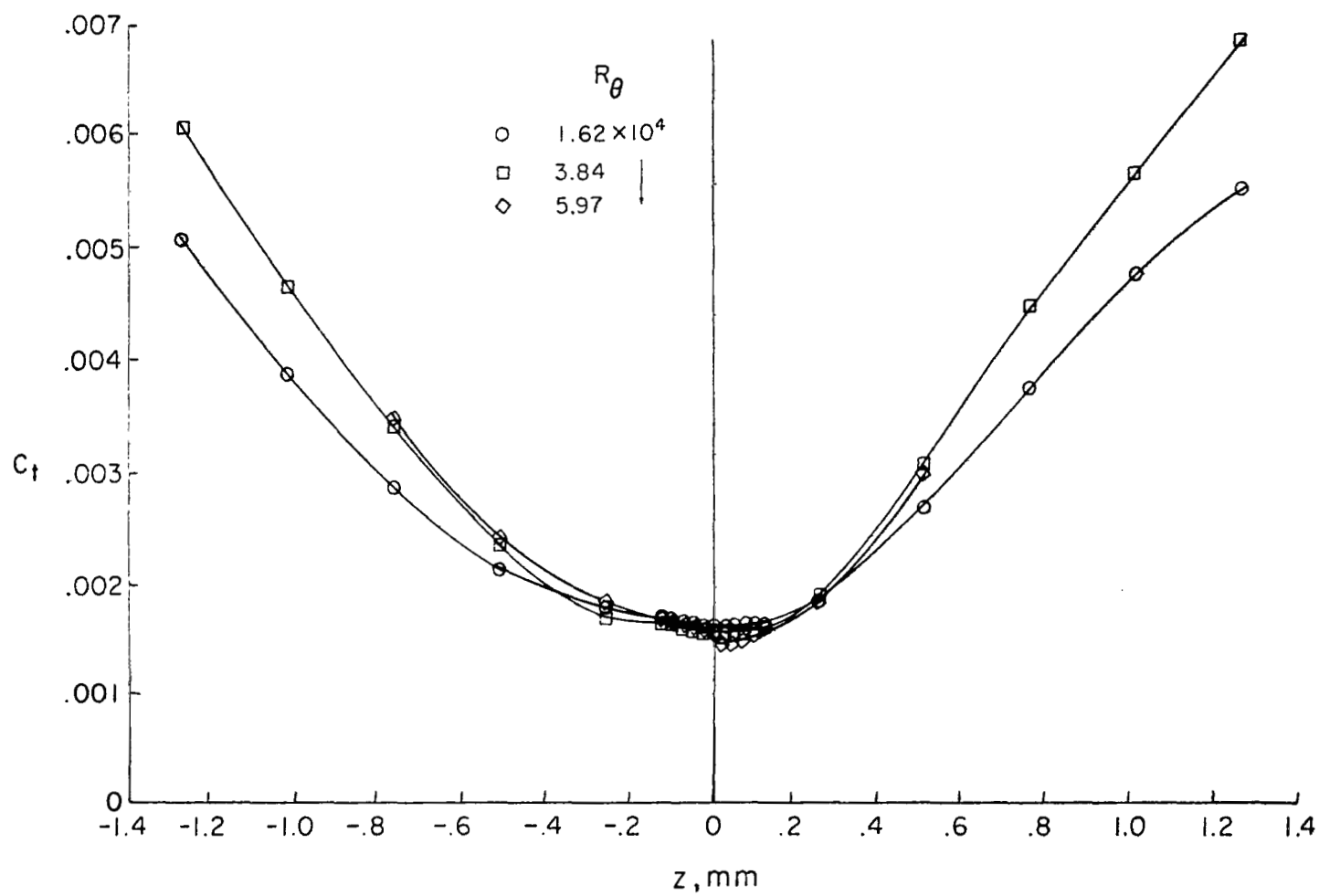
(d) G/D = 0.006.

Figure 5.- Continued.
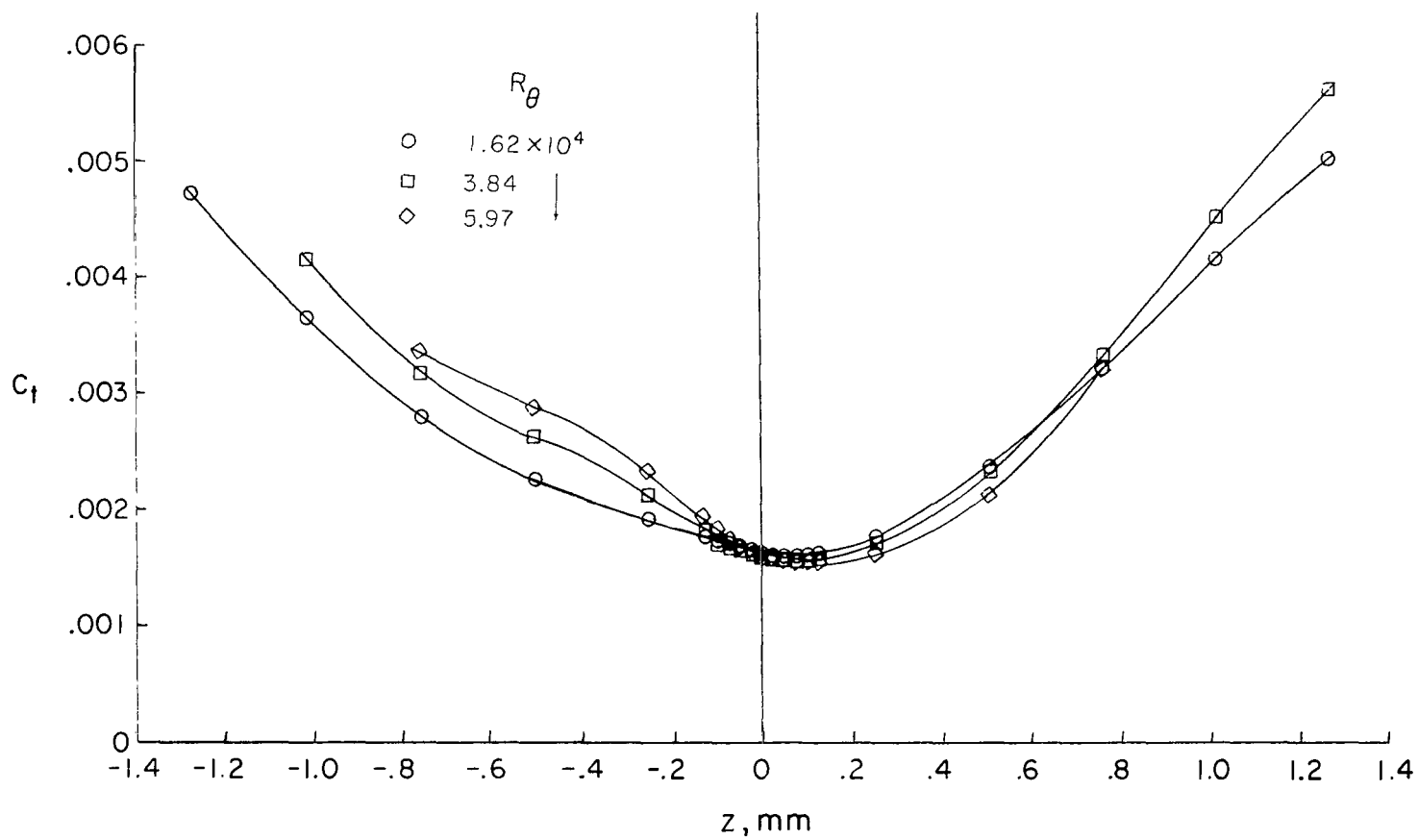
(e)   G/D □ 0.008.

Figure 5.- Continued.
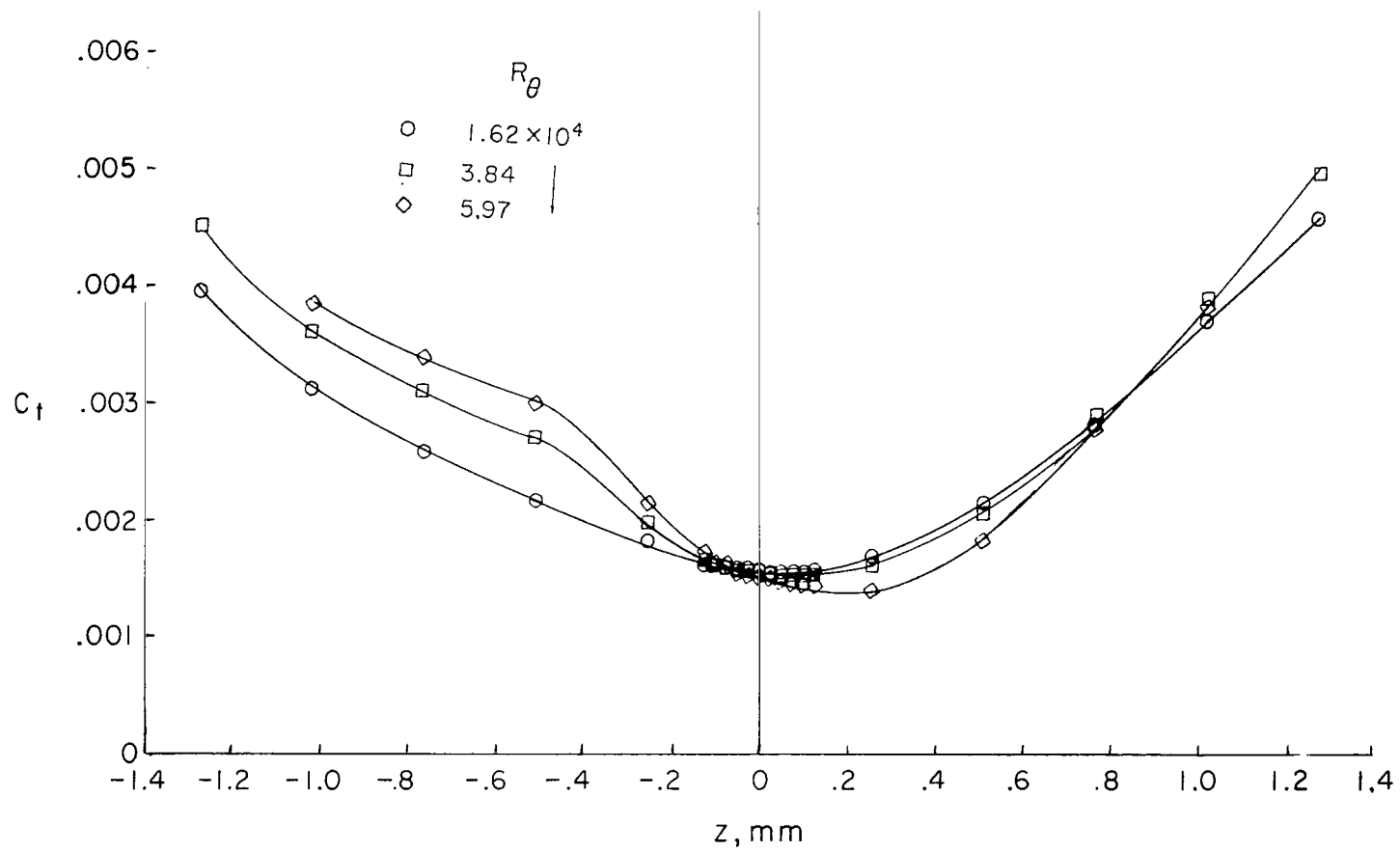
(f) G/D = 0.010.

Figure 5.- Concluded.
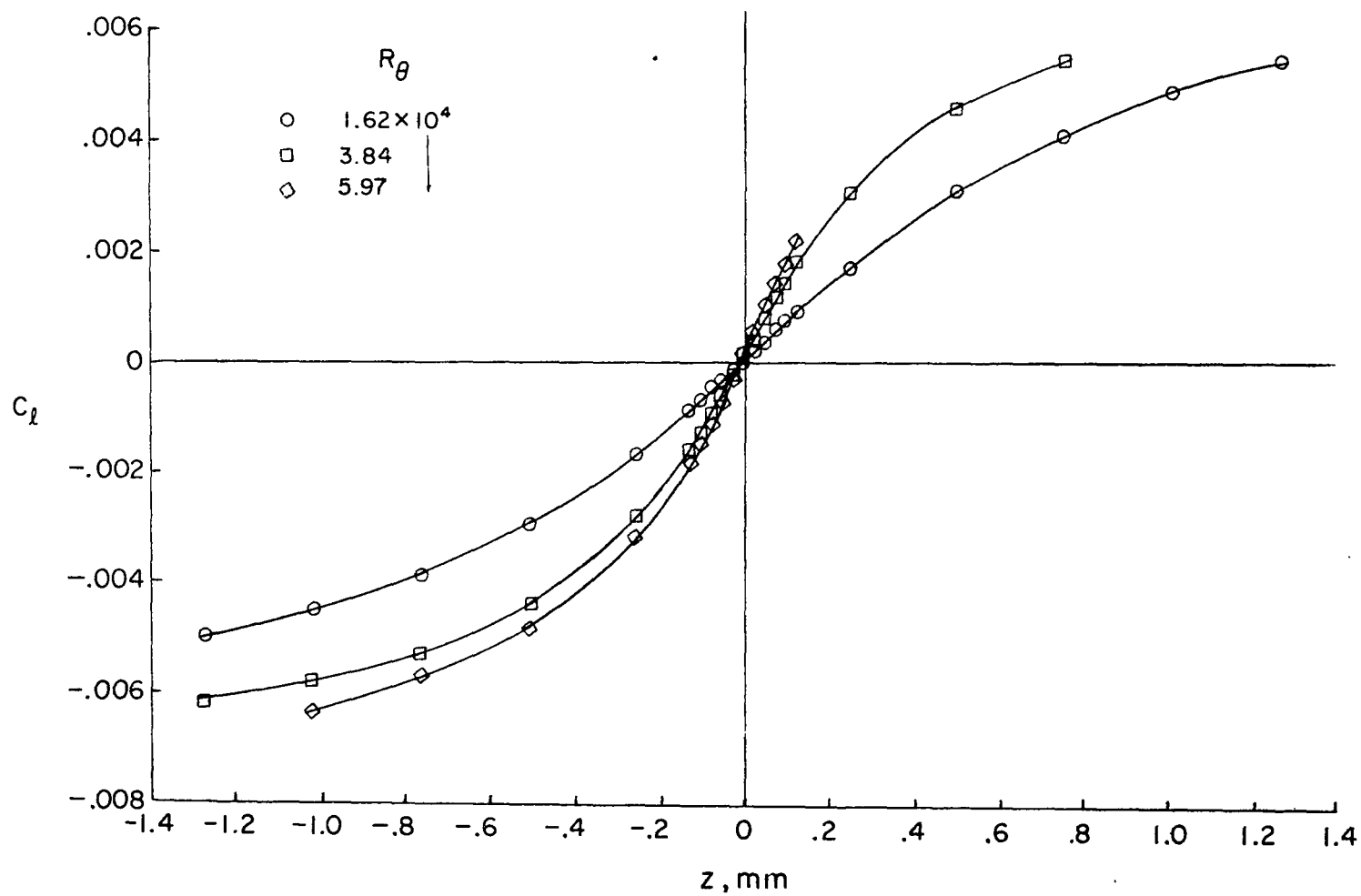
(a) G/D $=$ 0.001.

Figure 6.- Lip force results.
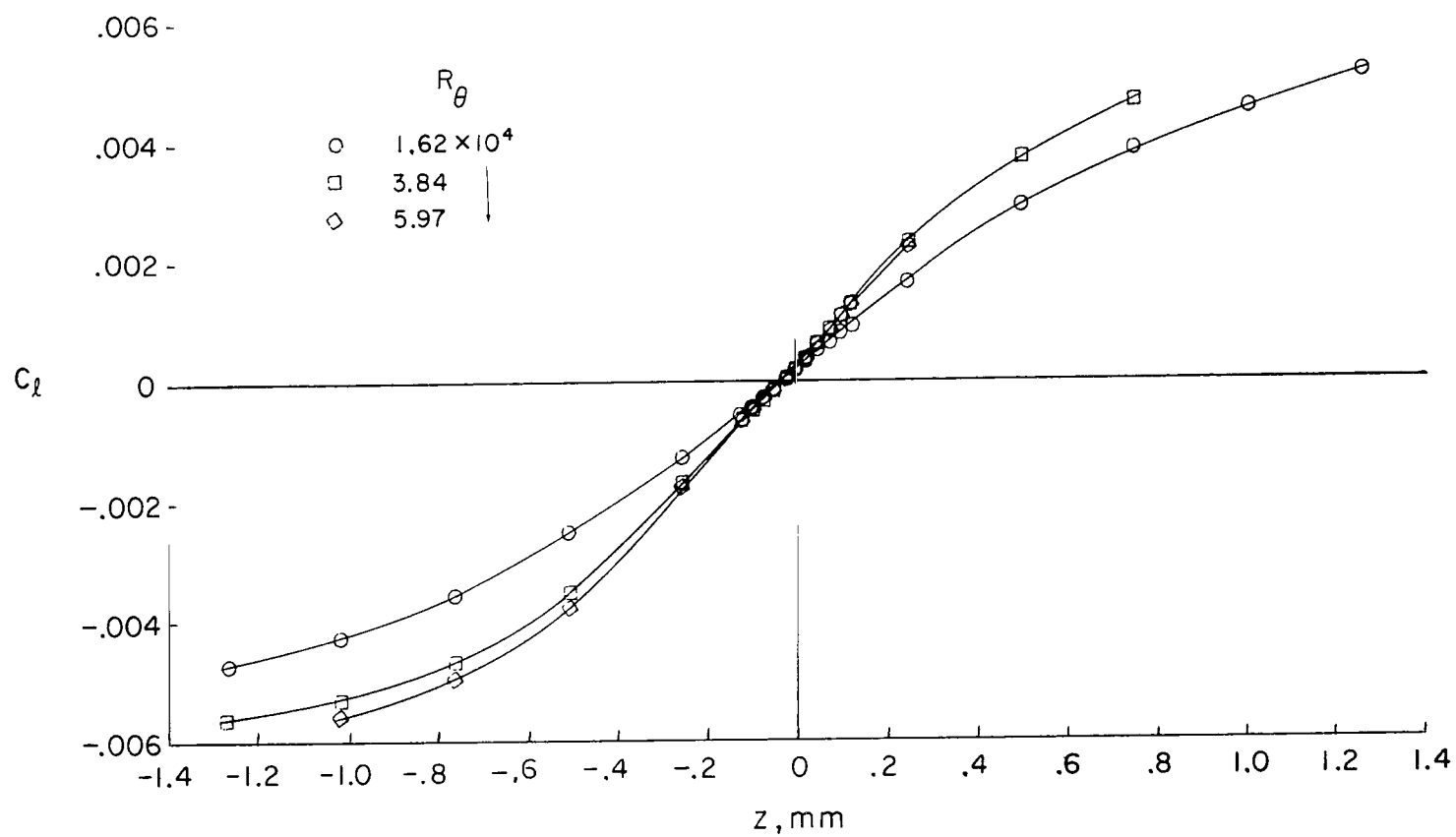
(b) G/D = 0.002.

Figure 6.- Continued.
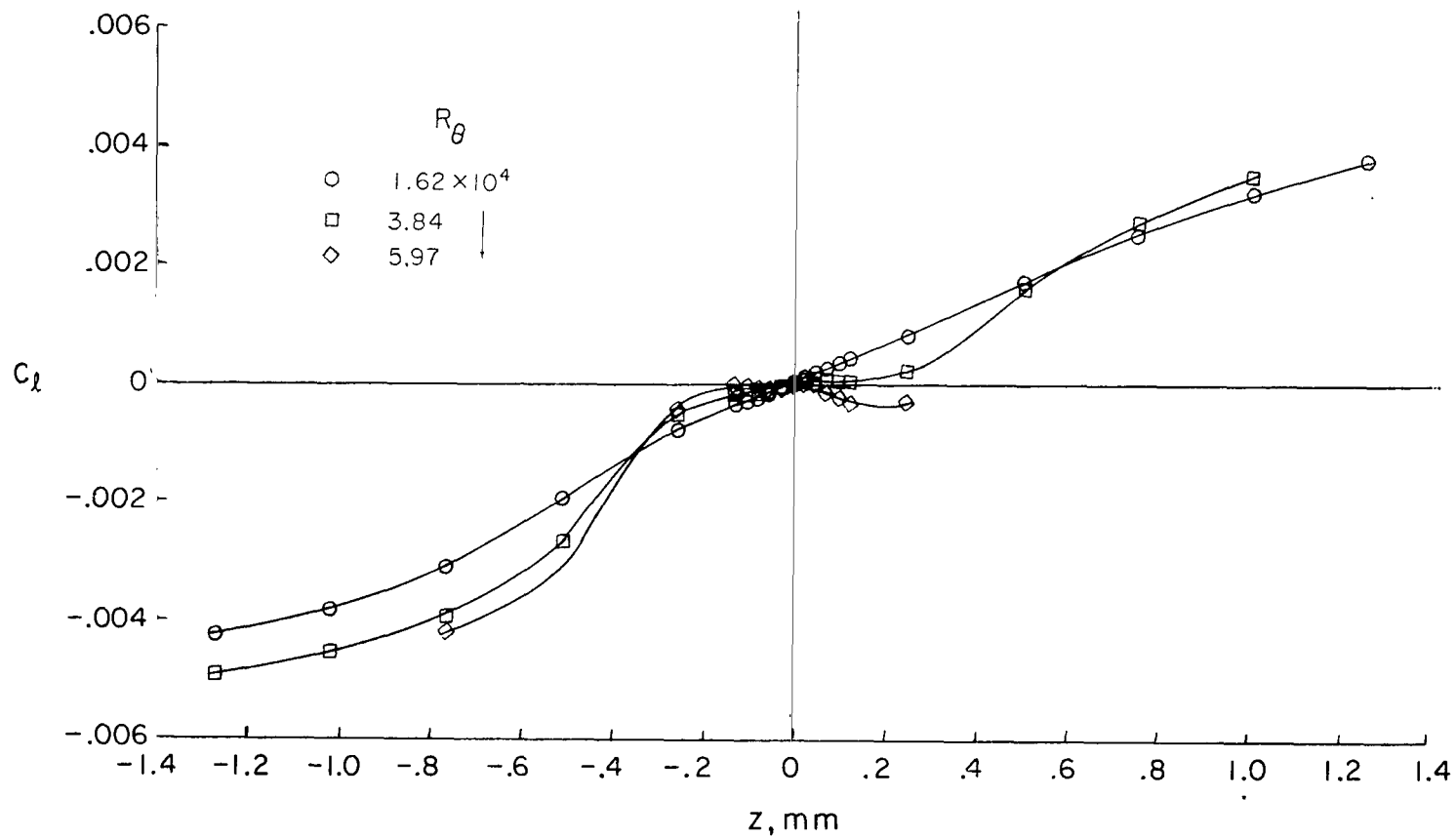
(c) G/D = 0.004.

Figure 6.- Continued.
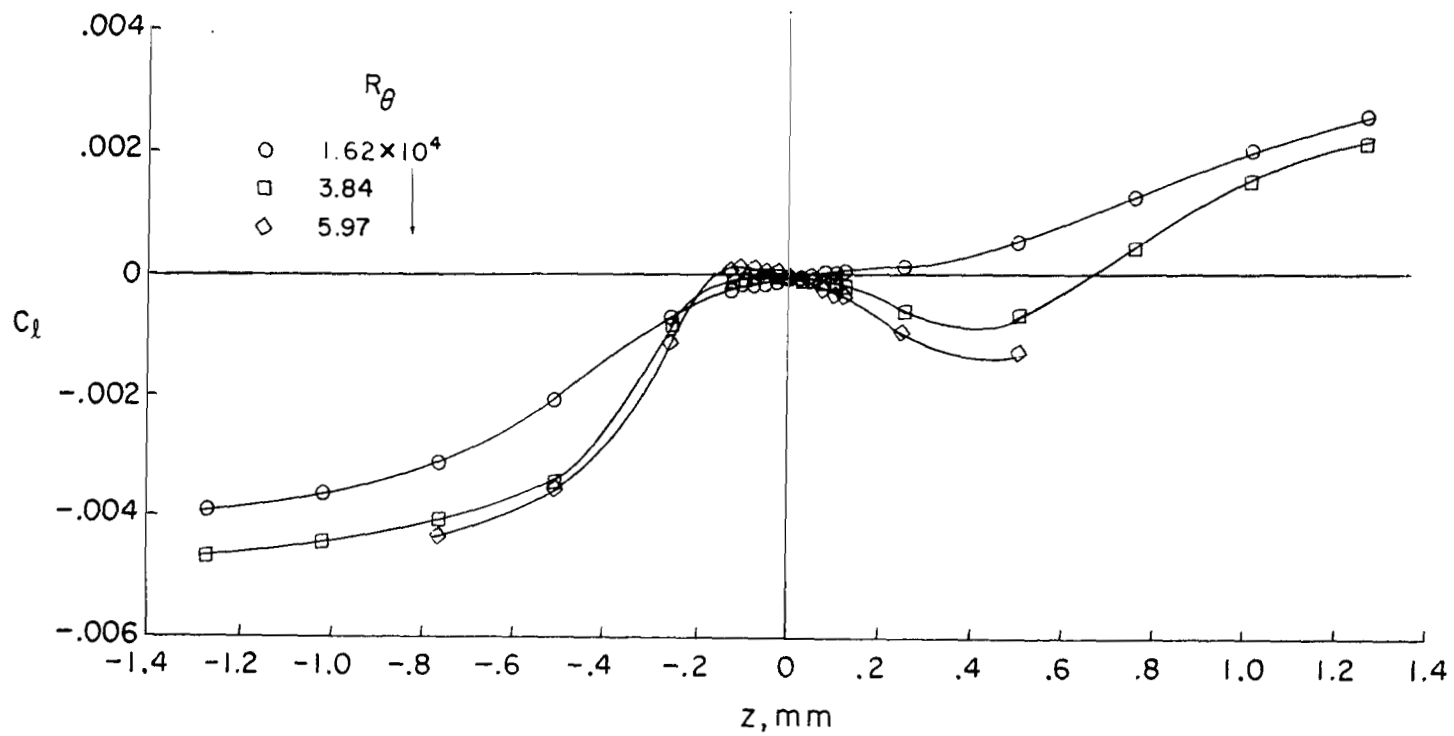
(d) G/D = 0.006.

Figure 6.- Continued.
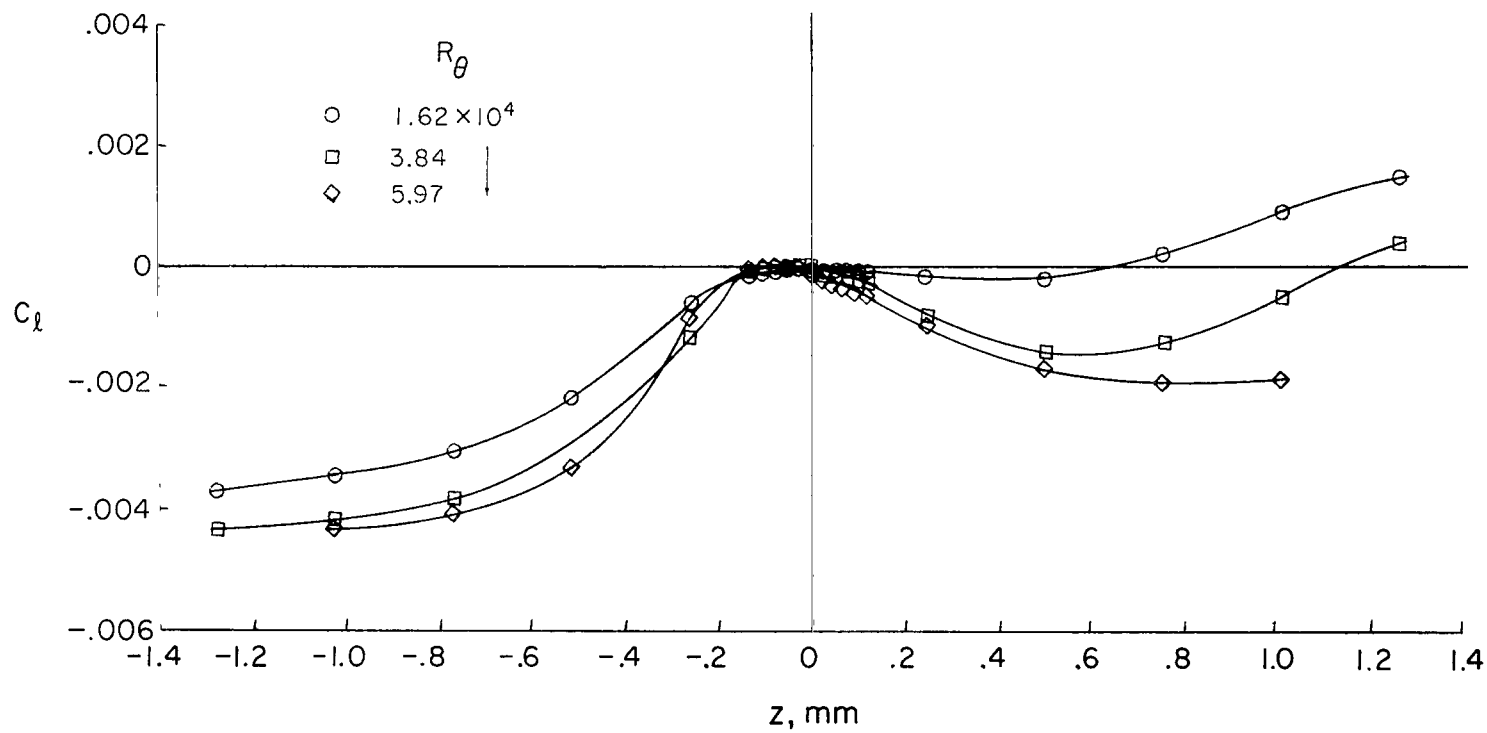
(e)   G/D = 0.008.

Figure 6.- Continued.
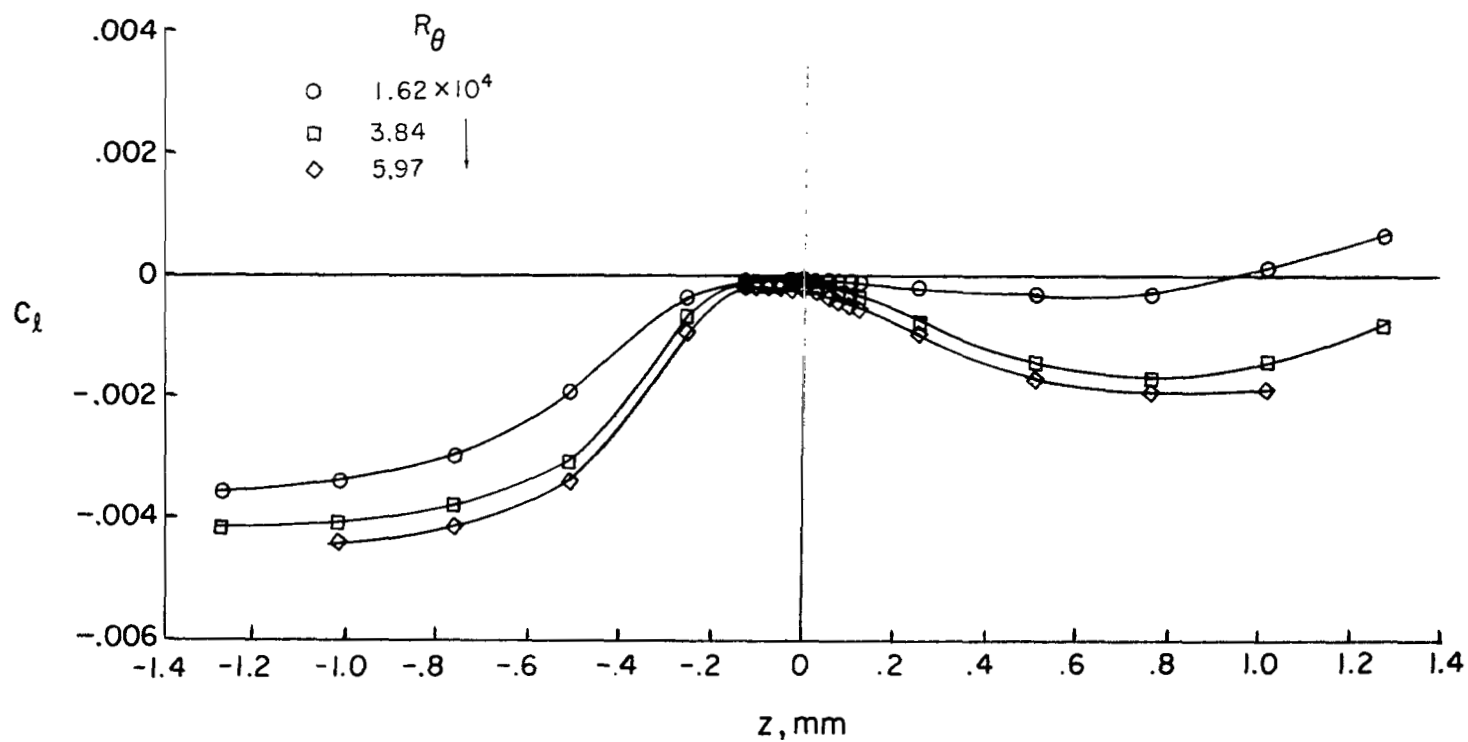
(f) G/D = 0.010.

Figure 6.- Concluded.
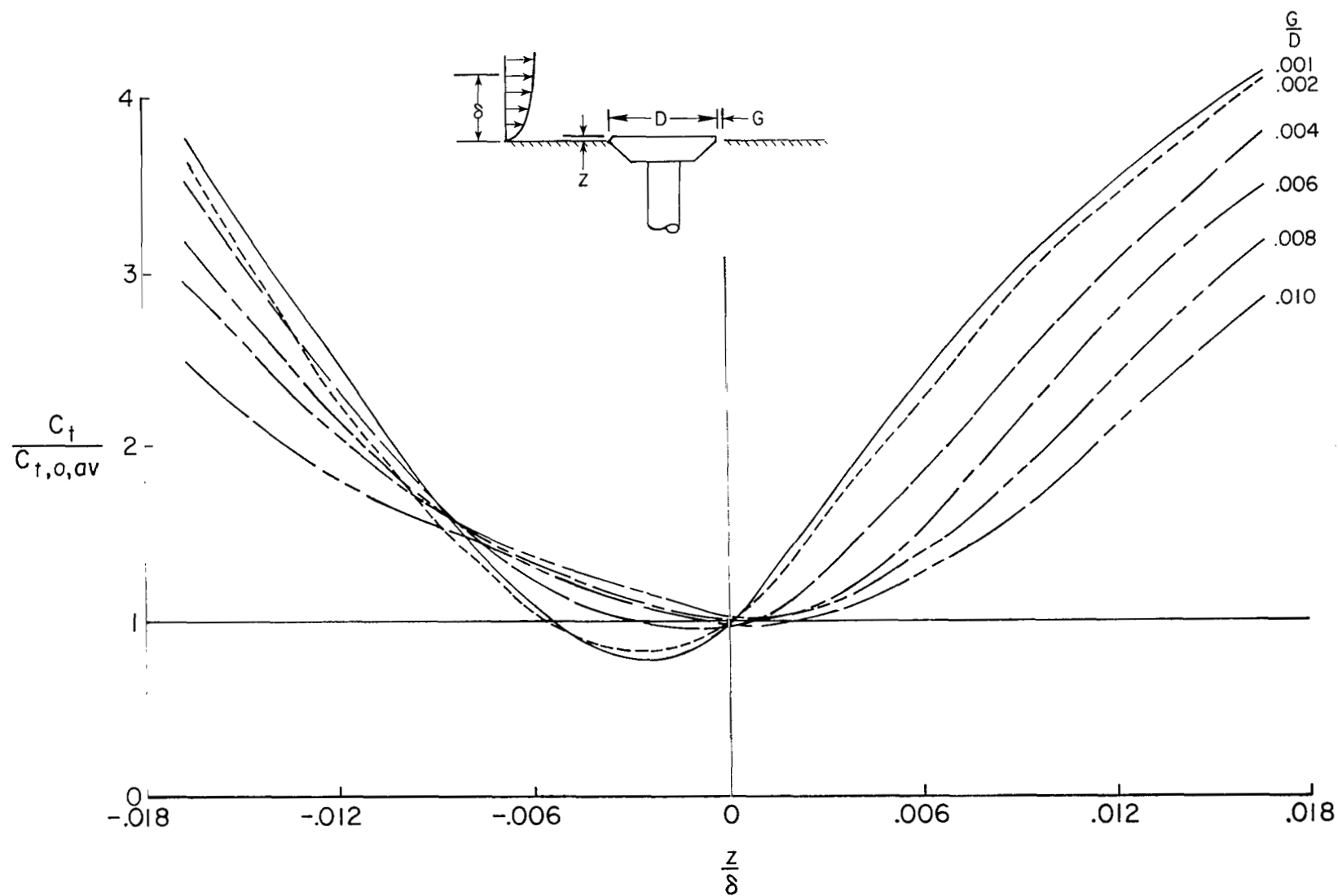
Figure 7.- Effect of protrusion and gap size on total force.

$$R_\theta = 1.62 \times 10^4.$$
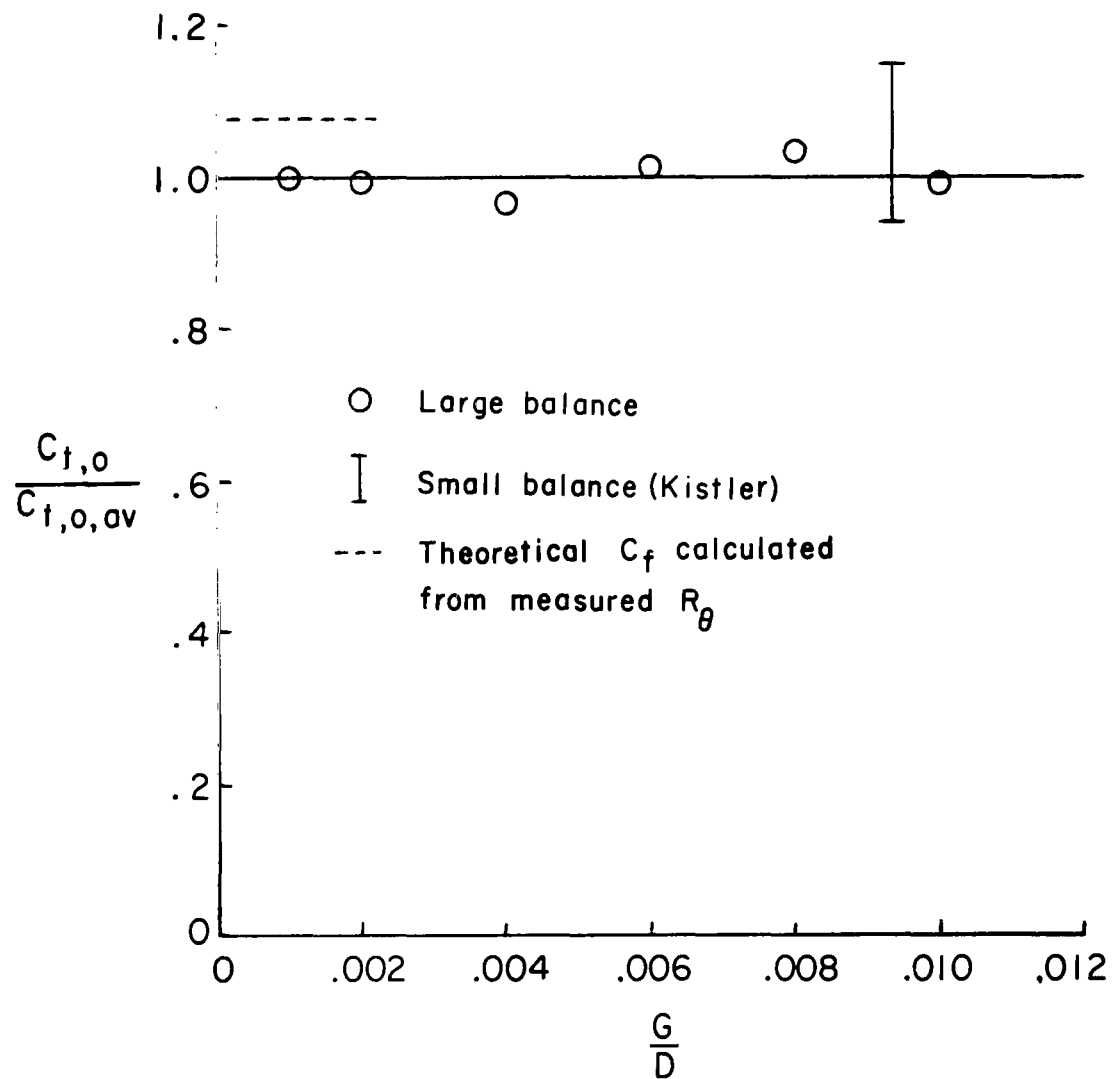
Figure 8.- Effect of gap size on total force at zero protrusion. $R_\theta = 1.62 \times 10^4$.
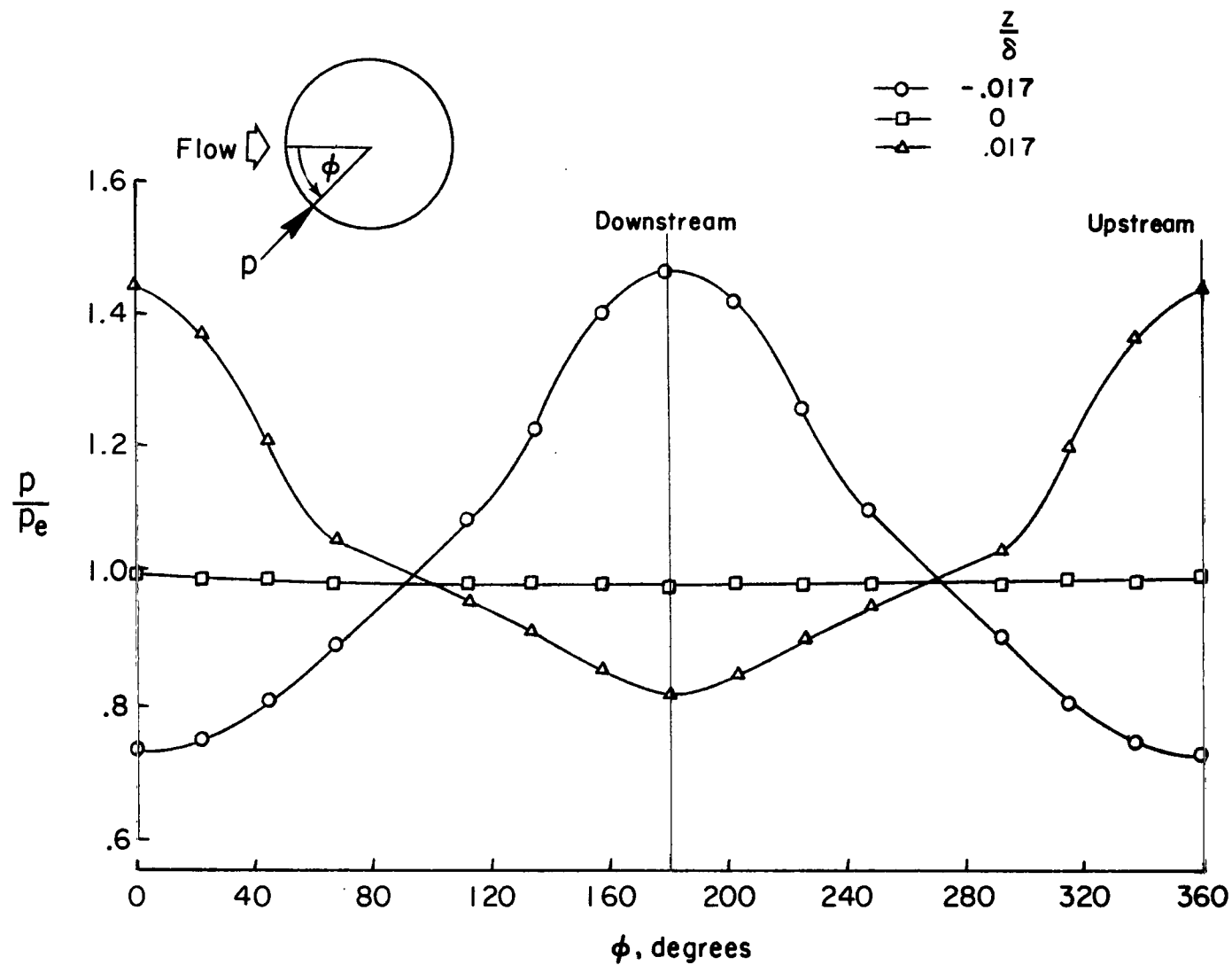
Figure 9.- Sample pressure distribution around lip for several protrusions. $R_\theta = 1.62 \times 10^4$; G/D = 0.001.
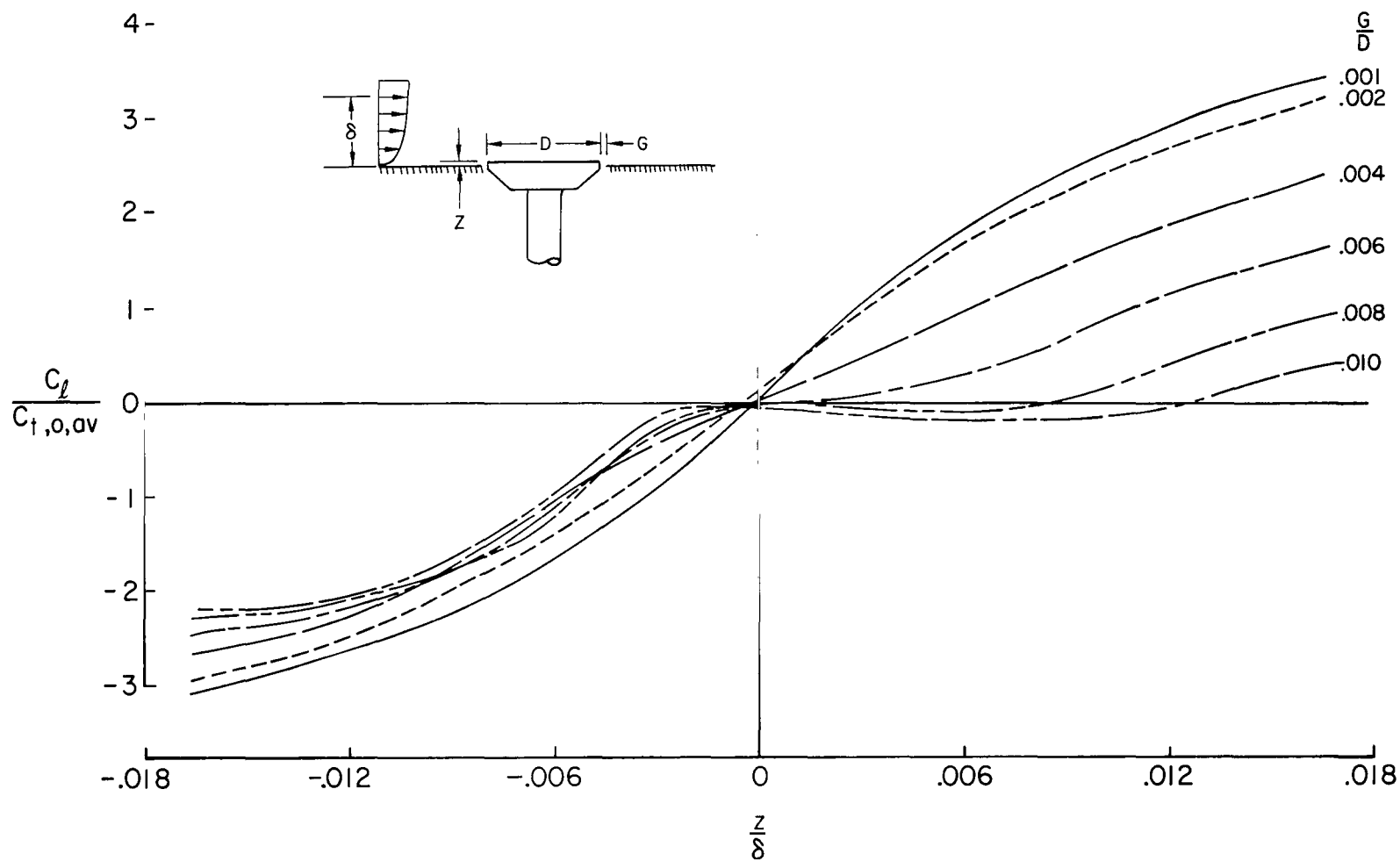
Figure 10.- Effect of protrusion and gap size on lip force.
$R_\theta = 1.62 \times 10^4$.
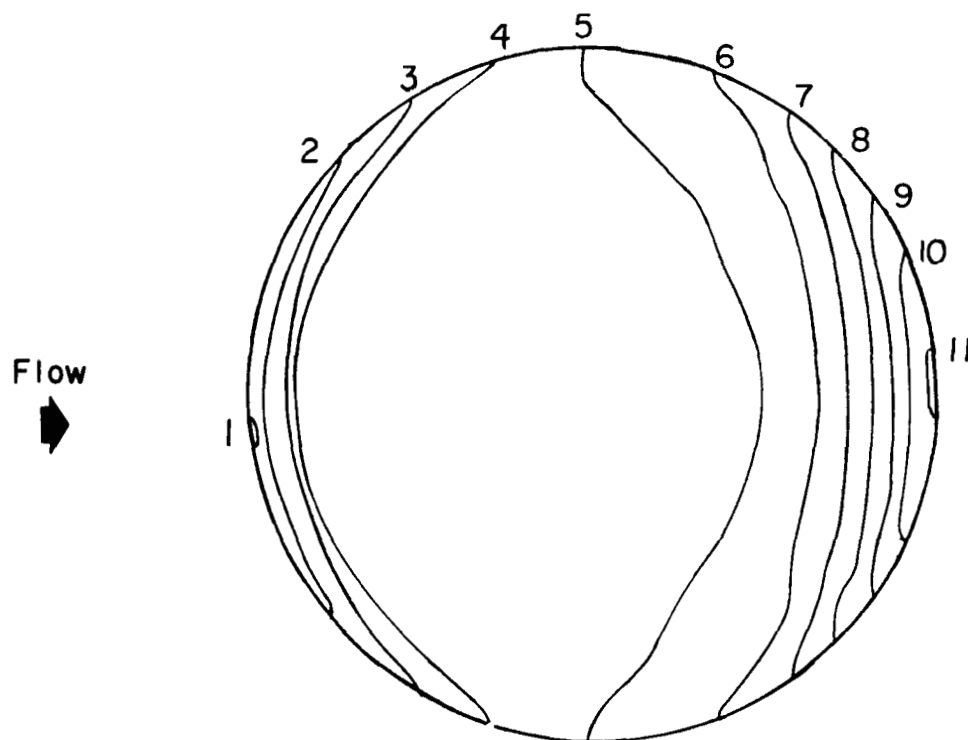
| Contour | p | | $\dfrac{p}{p_e}$ |
No.	N/m^2	psf	
1	2394	50	0.735
2	2633	55	0.809
3	2873	60	0.882
4	3112	65	0.956
5	3352	70	1.029
6	3591	75	1.103
7	3830	80	1.176
8	4070	85	1.250
9	4309	90	1.324
10	4549	95	1.397
11	4788	100	1.471

Figure 11.- Sample pressure contours on element surface.

$R_\theta = 1.62 \times 10^4$; $G/D = 0.001$; $z/\delta = -0.017$.
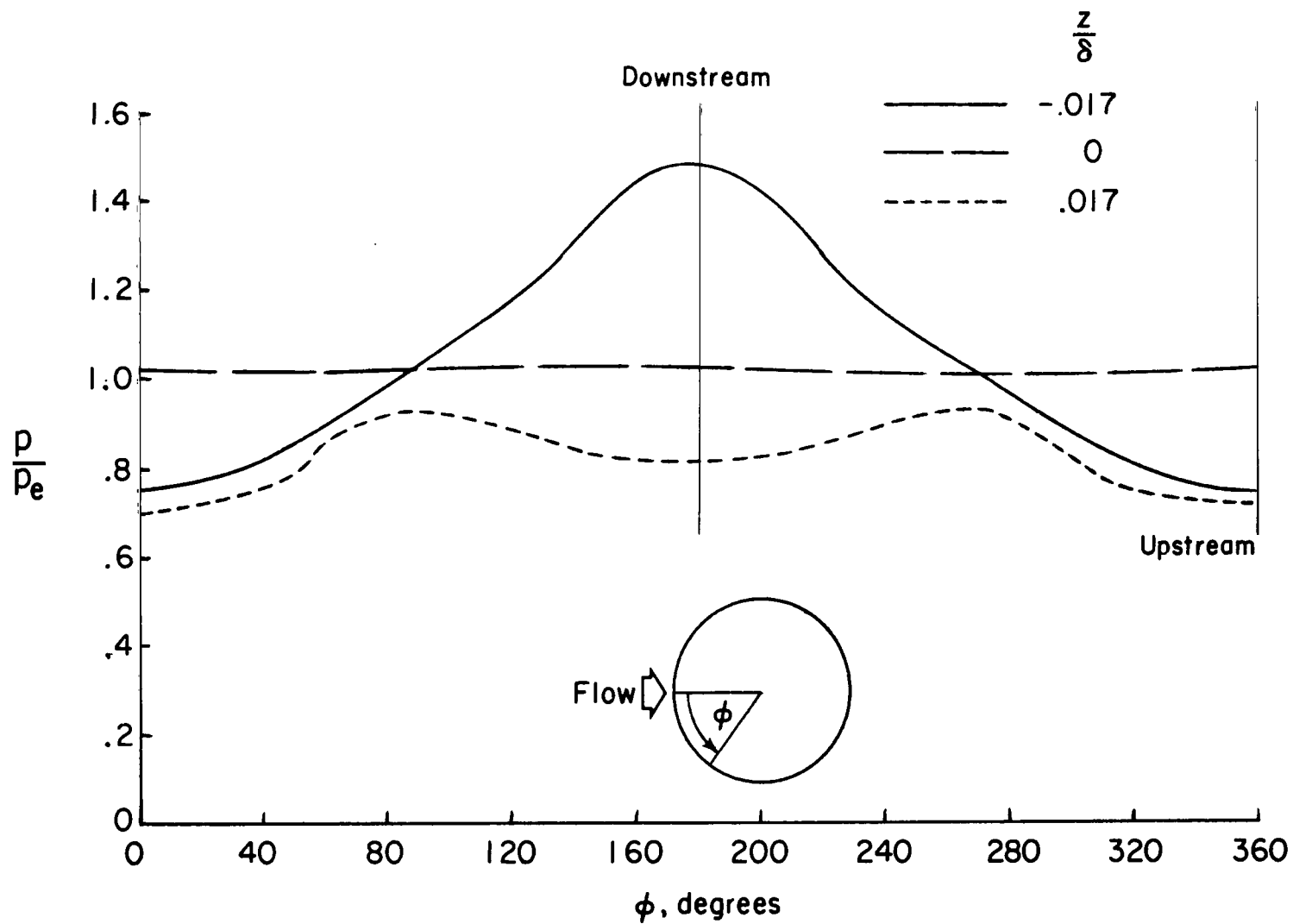
Figure 12.- Sample pressure distribution around edge of element surface for several protrusions. $R_\theta = 1.62 \times 10^4$; $G/D = 0.001$.
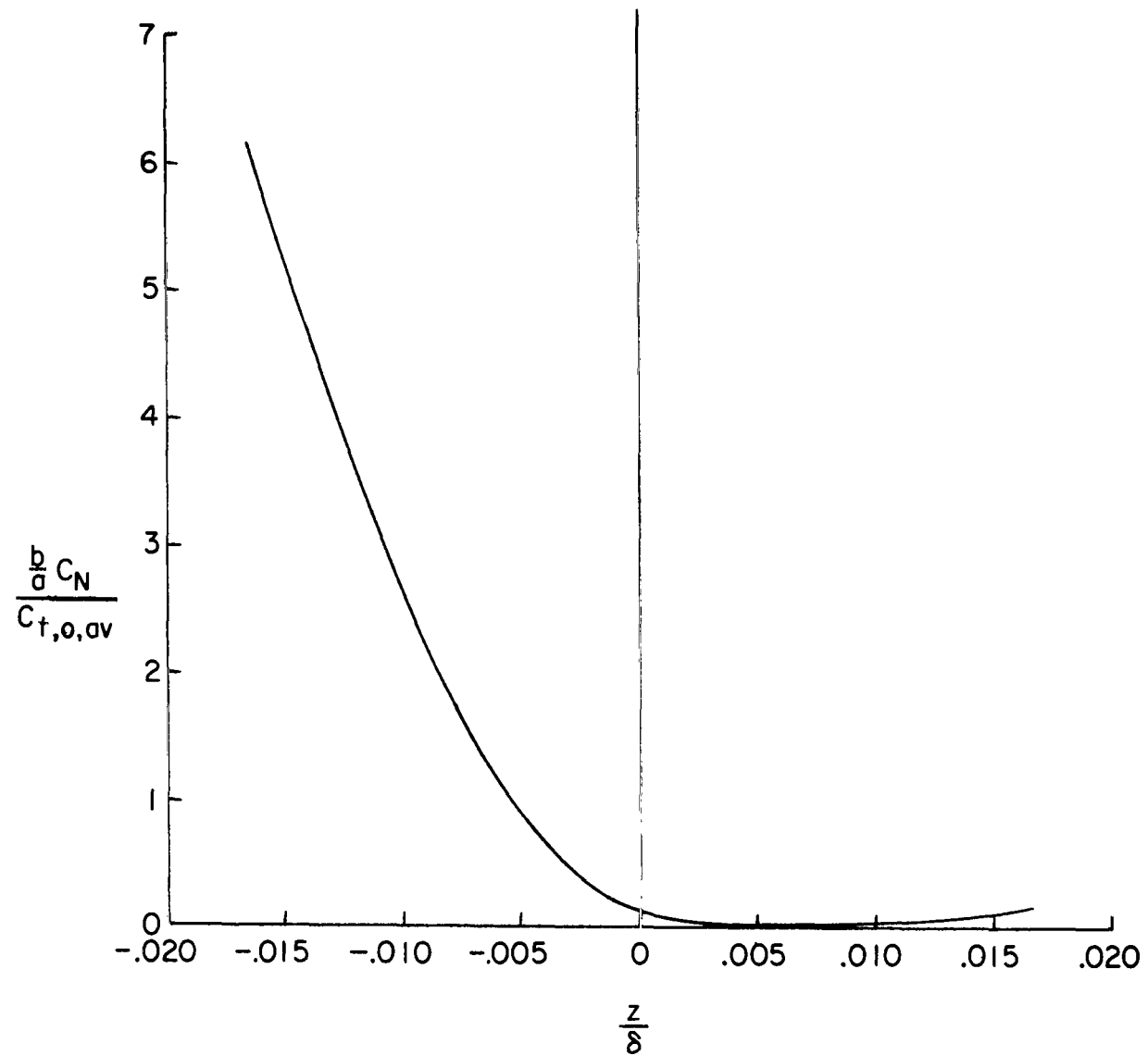
Figure 13.- Effect of protrusion on normal force contribution to balance output. $R_\theta = 1.62 \times 10^4$; $G/D = 0.001$.
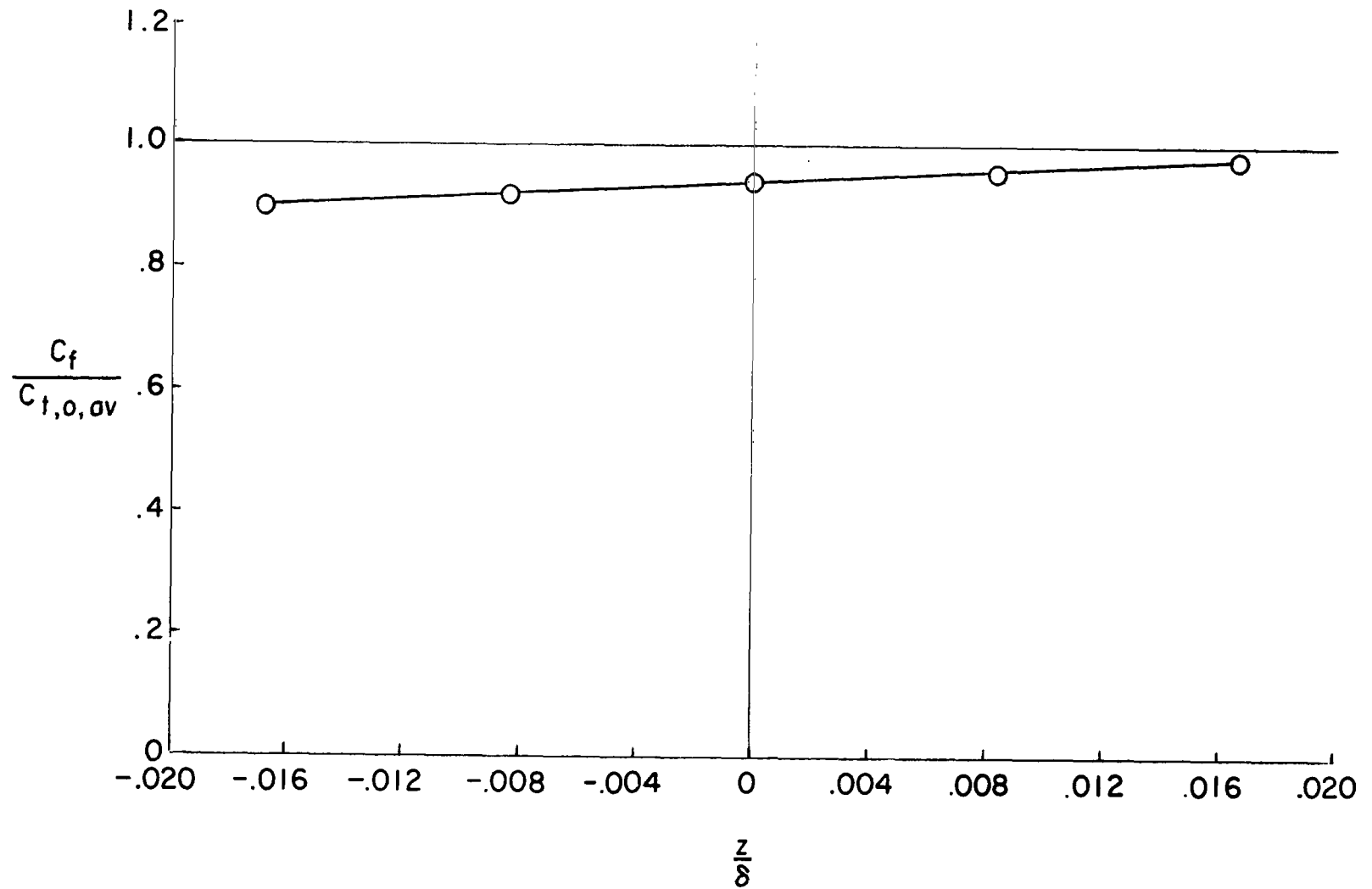
Figure 14.- Effect of protrusion on Preston tube skin friction.
$R_\theta = 1.62 \times 10^4$; $G/D = 0.001$.

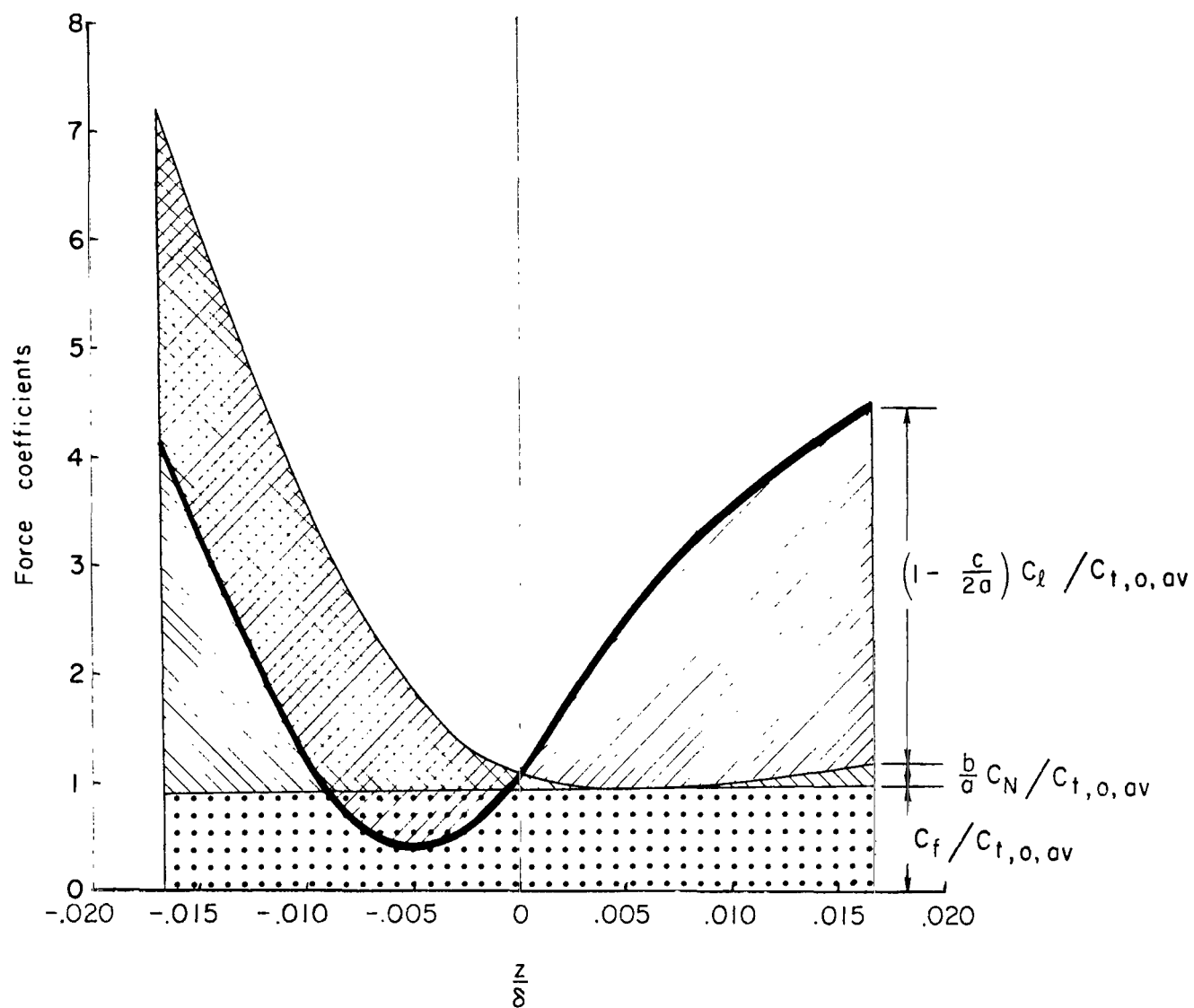Figure 15.- Comparison of friction, normal, and lip force contributions to total balance output. $R_\theta = 1.62 \times 10^4$; $G/D = 0.001$.
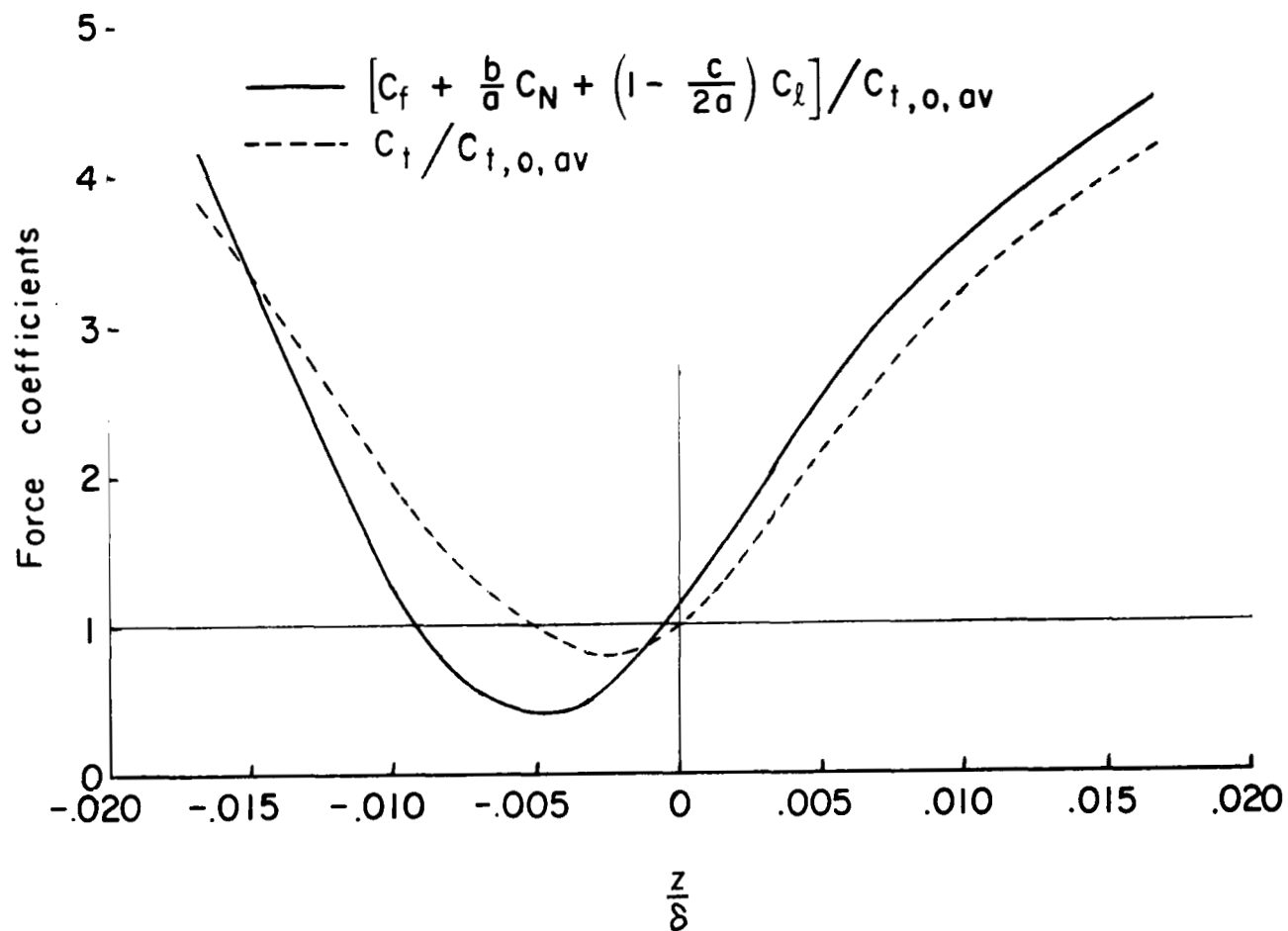
Figure 16.- Comparison of direct balance measurement with sum of friction, lip, and normal force measurements. $R_\theta = 1.62 \times 10^4$; $G/\dot{D} = 0.001$.
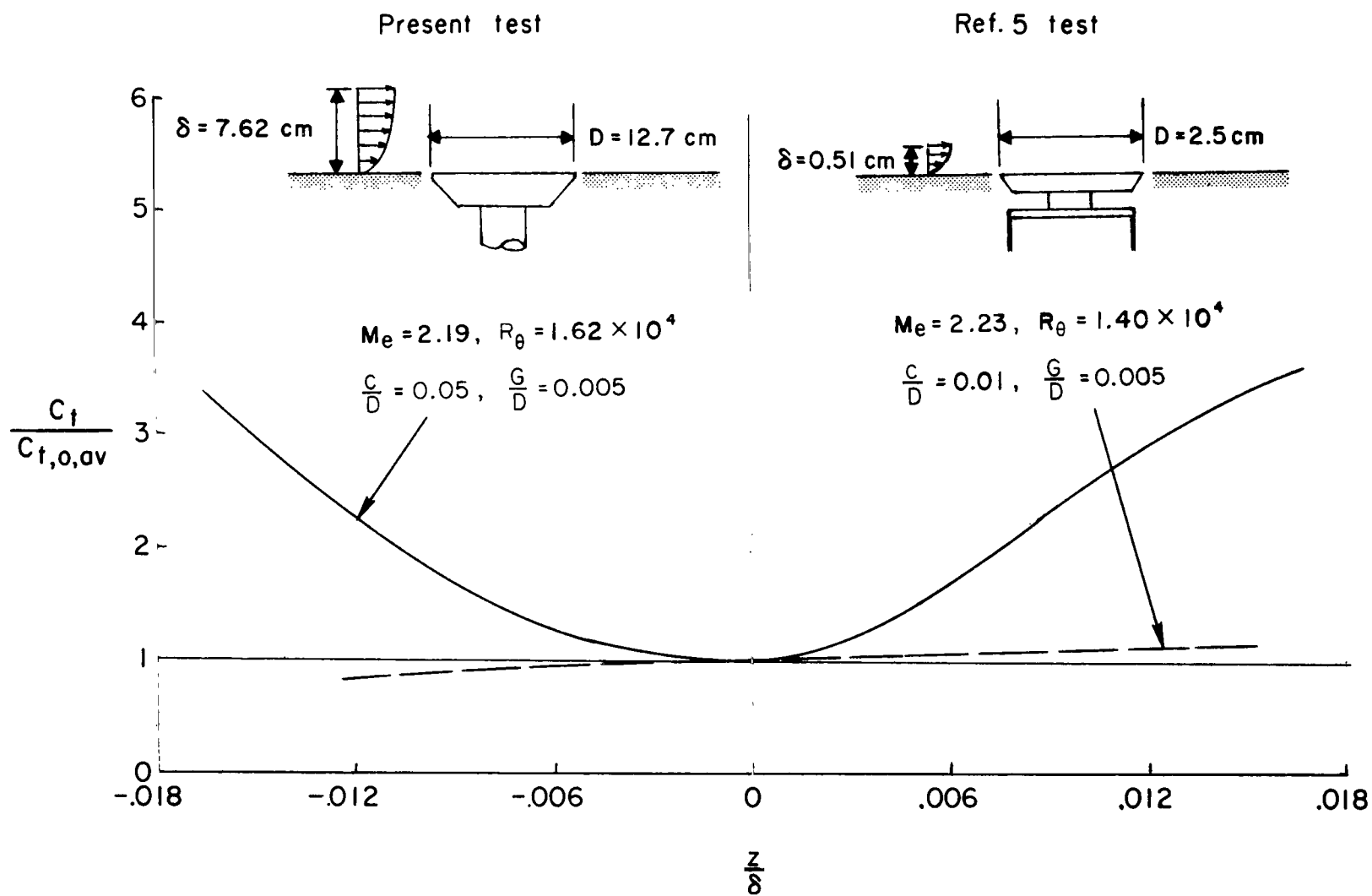
Figure 17.– Comparison between protrusion results of present investigation and that of reference 5.

"The aeronautical and space activities of the United States shall be conducted so as to contribute . . . to the expansion of human knowledge of phenomena in the atmosphere and space. The Administration shall provide for the widest practicable and appropriate dissemination of information concerning its activities and the results thereof."
—NATIONAL AERONAUTICS AND SPACE ACT OF 1958

NASA SCIENTIFIC AND TECHNICAL PUBLICATIONS

TECHNICAL REPORTS: Scientific and technical information considered important, complete, and a lasting contribution to existing knowledge.

TECHNICAL NOTES: Information less-broad in scope but nevertheless of importance as a contribution to existing knowledge.

TECHNICAL MEMORANDUMS: Information receiving limited distribution because of preliminary data, security classification, or other reasons. Also includes conference proceedings with either limited or unlimited distribution.

CONTRACTOR REPORTS: Scientific and technical information generated under a NASA contract or grant and considered an important contribution to existing knowledge.

TECHNICAL TRANSLATIONS: Information published in a foreign language considered to merit NASA distribution in English.

SPECIAL PUBLICATIONS: Information derived from or of value to NASA activities. Publications include final reports of major projects, monographs, data compilations, handbooks, sourcebooks, and special bibliographies.

TECHNOLOGY UTILIZATION PUBLICATIONS: Information on technology used by NASA that may be of particular interest in commercial and other non-aerospace applications. Publications include Tech Briefs, Technology Utilization Reports and Technology Surveys.

Details on the availability of these publications may be obtained from:

SCIENTIFIC AND TECHNICAL INFORMATION OFFICE

NATIONAL AERONAUTICS AND SPACE ADMINISTRATION
Washington, D.C. 20546